Formation and growth of diapirs in contractional settings: the Mediano anticline and Clamosa diapir case study (Southern Pyrenees)

Pablo Santolaria[1], Roi Silva-Casal[1], Núria Carrera[1], Josep A. Muñoz[1], Pau Arbués[1], Pablo Granado[1]

5   [1]Institut de Recerca Geomodels, Departament de Dinàmica de la Terra i de L'Oceà, Universitat de Barcelona (UB), C/Martí i Franquès s/n 08028 Barcelona, Spain.

Correspondence to: Pablo Santolaria (p.santolaria.otin@ub.edu)

Abstract. At the northwestern termination of the South Pyrenean Central Salient, thrust imbrication, detachment folding and diapirism are structurally and genetically related. The La Fueba imbricate system has been folded by the Mediano

10   detachment anticline, while this fold connects with the Clamosa diapir. Together, this structural-stratigraphic trinity provides an excellent example to evaluate the factors controlling purely contractional diapirs in onshore-offshore contractional fold-thrust systems. Our study integrates detailed geological mapping, a large structural dataset, new biostratigraphic data, and interpretations of well-tied depth-converted seismic lines and cross-sections. A combined evolutionary model for contractional diapir formation and evolution is presented. While less common than in extensional settings, the interplay

15   shortening of a salt horizon along with vertical axis rotations and local stretching and erosion of the overburden can lead to purely contractional salt diapirs.

1 Introduction

Salt-detached fold-and-thrust belts feature a common structural style characterized by low taper angles and regularly-spaced folds and thrusts (Davis and Engelder, 1985). Folds are usually symmetrical, upright, elongated, and display a regular

20   wavelength (e.g., Davis and Engelder, 1985; Harrison, 1995; Rowan and Vendeville, 2006). Salt thickness is a primary factor in determining the type of fold: a thicker salt than its overburden promotes the formation of salt-cored detachment folds, whereas thinner salt leads to thrusted folds (Stewart, 1999). Besides, the ratio of décollement thickness to cover thickness and the décollement strength (i.e., viscosity) control the structural spacing, fold amplitude, wavelength, and structural facing (e.g. Cotton and Koyi, 2000; Costa and Vendeville, 2002; Soto et al., 2002; Ruh et al., 2012). On the other

25   hand, sedimentation-erosion processes localize deformation and promote fold amplification (e.g. Storti and McClay, 1995; Mugnier et al., 1997; Pichot and Nalpas, 2009; Fillon et al., 2013; Duerto and McClay, 2009; Izquierdo-Llavall et al., 2018; Pla et al., 2019). It must be borne in mind that these factors can vary both spatially and temporally, and so may the associated structural styles and kinematics.

Many salt-detached fold-and-thrust belts include salt diapirs, such as in the Fars province area in the Zagros fold-belt (e.g. Jahani et al., 2009; Callot et al., 2012; Snidero et al., 2020), the Hellenides (e.g., Velaj et al., 2002; Vakalas et al., 2023), the SW Sub-Alpine chains (e.g. Célini et al., 2020), the Atlas Mountains (e.g. Saura et al., 2014; Calvín et al., 2018; Casas-Sainz et al., 2023), the Betic Cordillera (e.g. Roca et al., 2006; Escosa et al., 2018; Flinch and Soto, 2022) and the Pyrenees (e.g.

35   Canérot et al., 2005; Muñoz et al., 2013; Santolaria et al., 2016), among others. In most cases, diapirs in such settings are inherited features, originating from extension, differential loading, or gravitational gliding on rifted margins predating contraction (e.g. Roca et al., 2006; Santolaria et al., 2022; Strauss et al., 2023). Upon shortening and due to the low-strength of salt, diapirs are easily rejuvenated (e.g. Vendeville and Nilsen, 1995; Callot et al., 2012; Dooley et al., 2009; Granado et al. 2019; Santolaria et al., 2021a) and commonly focus deformation and localize contractional structures (e.g. Rowan and

40   Vendeville, 2006; Santolaria et al., 2021b). In the absence of inherited salt structures, diapirism in fold-and-thrust belts is less common (Vendeville and Jackson, 1992; Jackson and Vendeville, 1994) and is hindered by factors such as: i) a relatively thick cover strengthened by horizontal contractional stresses, ii) a relatively thin décollement (i.e., the salt budget limiting factor), iii) predominance of thrusting over folding, and iv) high syn-contractional sedimentary rates (Bonini, 2003; Barrier et al., 2013) (Fig. 1a). Therefore, triggers and processes that enhance diapirism in such settings include: i) a relatively

45   thin cover over a thick salt décollement, ii) folding rather than thrusting, iii) low to moderate syn-contractional sedimentary rate relative to uplift, thus favouring erosion (Sans and Koyi, 2001), v) lateral gradients of thrust displacement accommodated with localized extension, vi) salt migration and inflation (Fig. 1b), vii) the presence of salt in the hanging wall of a thrust carried up to shallow levels where it can break through to the surface (Rowan, 2020), viii) salt breaking through the thin roof of an early salt-cored anticline or the thick roof of a later fold that is thinned by erosion (Coward &

50   Stewart, 1995). What are then the feedbacks and necessary balance between unfavourable and favourable factors critical for the occurrence of diapirism and its subsequent enhancement or inhibition?
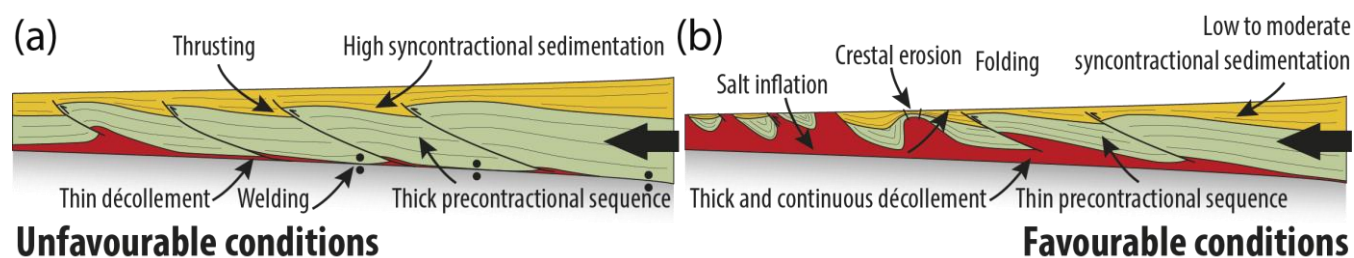
Figure 1: Summary sketches that illustrate unfavorable (A) and favorable (B) conditions for the development of purely contractional diapirs in fold-and-thrust belts.

55

In this contribution, we present the South Pyrenean Central Salient as a unique scenario due to the outstanding preservation of syn-contractional growth strata and the available subsurface data surrounding several salt bodies. Our analysis assesses the feedbacks and balance between diapirism triggers and inhibiting factors and processes (e.g., Muñoz et al., 2024). We illustrate these dynamics trough a detailed case study of the Clamosa diapir, a Triassic salt body surrounded by pre-, syn-,

60   and post-tectonic units (Fig. 2), along with nearby contractional structures: the Mediano detachment anticline, and the La
      Fueba imbricate thrust system. Our methodology included constructing a detailed new geological map completed based on
      our own fieldwork and the synthesis of previous geological maps (Arbués and Corregidor, 1995; Arbués et al., 2007;
      Fernández et al., 2004; Teixell and Barnolas, 1995; Gomis et al., 2012; Garrido-Megías, 1973; Poblet et al., 1998; Barnolas
      et al., 1994b). This surface geology work is complemented by constructing and analysing serial cross-sections integrated
65   with and supported by well-tied depth-converted 2D seismic data. In addition, our structural-kinematic evolutionary model is
      supported by new biostratigraphy dating based on foraminifera content from key localities. Our proposed model is framed
      within the regional context of the South Pyrenean Central Salient (Muñoz et al., 2018, 2024). Additionally, we evaluate and
      discuss the factors that determine the formation of salt diapirs in fold-and-thrust belts, and their connection with adjacent
      non-diapiric structures, such as detachment anticlines and thrust imbricates.

70

2. Geological setting

2.1. The South-Central Pyrenees

75   The Pyrenean mountain range formed as a result of the collision between the Eurasian and Iberian plates from Late
      Cretaceous to Miocene times, resulting in the growth of an asymmetric doubly-vergent orogenic wedge (Roest and
      Srivastava, 1991; Rosenbaum et al., 2002). This collision involved the subduction of the Iberian lower crust attached to its
      lithospheric mantle beneath the European Plate (Choukroune, 1989; Muñoz, 1992; Pedreira et al., 2003; Campanyà et al.,
      2012; Chevrot et al., 2015, 2018), and the inversion of the Late Jurassic-Early Cretaceous rifted margin (Mencós et al. 2015;
80   Muñoz et al. 2018). The Pyrenean structural style is thus mainly controlled by the inversion of inherited features but also by
      the distribution of the Triassic evaporites and shales, which acted as the regional thin-skinned décollement in the Southern
      Pyrenees. The South-Central Pyrenees form a thrust salient (Fig. 2) whose curvature developed by the progressive bending
      resulting from divergent thrust transport directions (Muñoz et al., 2013; 2024). Preservation of syntectonic sediments since
      the early stages of convergence provides constraints on the thrusts' sheets kinematics of the salient. From north to south, and
85   older to younger, these thrust sheets are: the Late Cretaceous Cotiella-Bóixols, the Paleocene-late Ypresian Peña Montañesa-
      Montsec, and the Lutetian-Oligocene Gavarnie-Sierras thrust sheets. Displacement of these thrust sheets was coeval with
      basement-involved thrusting in the Axial Zone (Séguret, 1972; Cámara and Klimowitz, 1985). In the Gavarnie-Sierras thrust
      sheet displacement is mainly accounted by several basement-involved thrusts, such as the Gavarnie, Bielsa and Guarga
      thrusts that mostly moved diachronously and in sequence (Séguret, 1972; Cámara and Klimowitz, 1985; Martínez-Peña and
90   Casas-Sainz, 2003). The Gavarnie thrust started to develop during early Lutetian times (the age of the onset of folding in its
      hanging wall, Séguret, 1972; Fernández et al., 2012; Muñoz et al., 2013), until it was tilted, folded, and piggy-back
      transported southwards since late Eocene times by the Guarga and related basement thrusts.
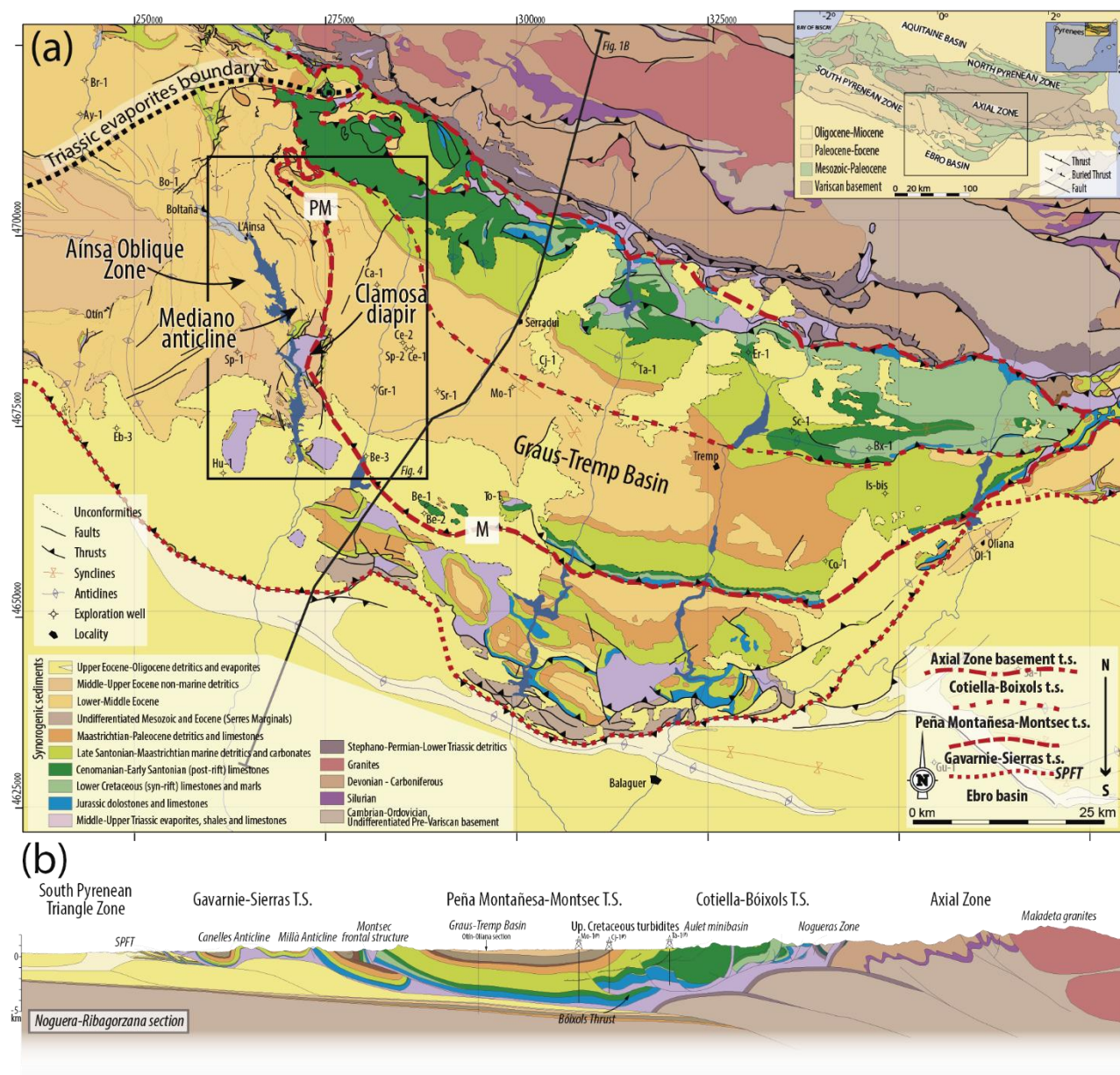
Figure 2. (a), Geological map of the South Pyrenean Central Salient. Dashed and dotted red lines represent the contact between the Axial Zone and the Southern Pyrenean fold and thrust belts and the Bóixols-Cotiella, Montsec-Peña Montañesa and Gavarnie-Sierras thrust sheets (modified from Muñoz et al., 2018 and Santolaria et al., 2024; inset map after Beamud, 2013). A black rectangle frames the studied area shown in Fig. 4. (b), Cross-section illustrates the western half of this Pyrenean Salient (from Santolaria et al., 2024). PM, Peña Montañesa thrust; M, Montsec thrust.

95

100

The studied area is on the western edge of the South Pyrenean Central Salient, where the N130E trending Montsec thrust turns into a N-S orientation to merge with the Peña Montañesa south-directed thrust system (Fig. 2). East of it, the Graus-Tremp basin extends to the east as the piggyback basin ridding on top of the Montsec thrust sheet (Fig. 2). West of it, the Mediano anticline and Clamosa diapir are the easternmost structures of a set of N-S trending folds that belong to the Aínsa Oblique Zone (Muñoz et al., 2013). Besides, the Clamosa diapir represents the northernmost diapir of those structures belonging to the Gavarnie-Sierras thrust sheet. Paleomagnetic and structural studies have revealed the N-S folds in the Gavarnie-Sierras thrust sheet originated slightly oblique to the Pyrenean main N120E trend and underwent syn- to post-folding clockwise vertical axis rotations during Eocene to Oligocene times (Mochales et al., 2012, Muñoz et al., 2013). A more detailed description of the geology of the area studied is provided in section 3.

2.2 Stratigraphic units

The stratigraphy of the studied area is summarized in the chronostratigraphic diagram of figure 3. Paleozoic rocks represent the base of the stratigraphic sequence, only outcropping in the Axial Zone antiformal stack to the north. Paleozoic basement was drilled at -4457 m.b.s.l. in the Huesca-1 exploration well, c. 20 km SSW of the Clamosa diapir (Fig. 4). In the Axial Zone, Paleozoic units are unconformably overlain by Permian - Lower Triassic red beds and a strongly mobile Middle-Upper Triassic layered evaporitic sequence of evaporites, shales, carbonates and minor dolorites which constitute the regional décollement of the Pyrenees. On top of this sequence, scarce bodies of Rhaetian to Lower Jurassic limestones and dolostones crop out or were drilled by exploration wells. Cretaceous rocks are represented by Cenomanian limestones and dolostones, Santonian to Campanian carbonates and Campanian to Maastrichtian limestones and calcareous sandstones. Paleocene rocks are constituted by continental mudstones and limestones (Garumn facies) that grade into marine limestones and dolostones to the northwest. Above, the lower Ilerdian (i.e., lower Ypresian) Alveolina Limestone (Mey et al., 1968) is overlain by a succession of Ilerdian marls and limestones. On top, Cuisian (i.e., upper Ypresian) carbonate platforms laterally grade into the lower part of the deep marine Aínsa slope complex deposits (Cuisian and Cuisian-Lutetian deep marine deposits, fig. 3) which were fed from the easterly fluvio-deltaic systems of the Tremp-Graus Basin (i.e., Ilerdian-Cuisian fluvio-deltaic systems). Among the latter, the Castissent Fm. (Nijman and Puigdefàbregas, 1978) represents a major fluvial progradation towards the studied area (Marzo et al., 1988).

During the Lutetian, east-sourced fluvio-deltaic systems (Fig. 3, e.g., Garrido-Megías, 1968; Nijman and Nio, 1975) in the vicinities of the Clamosa diapir were topped by the deltaic Pano Fm. (Donsellar and Nio, 1982). These fluvio-deltaic systems include a succession of fluvial mudstones, sandstones and conglomerates that grades westwards to prodelta fossiliferous sandstones and mudstones and interbedded carbonate platform and reef limestones. These interbedded carbonates are found as isolated patches likely related to localized highs along the eastern and southwestern limbs of the Clamosa diapir. Eventually and especially in the western flank of the Clamosa diapir, a carbonate breccia unconformably overlies Upper

135   Cretaceous and locally represent the base of the fluvio-deltaic sequence. Carbonate breccia is essentially made of Upper-Cretaceous sub-rounded clasts in a sandy matrix containing foraminifera and its thickness varies from few tens centimeters to few meters. On top of the fluvio-deltaic deposits, the Pano Fm. is constituted by nearshore sandstones to deep-water mudstones organized in a transgressive sequence which also locally includes carbonate platforms. Fluvio-deltaic systems grade laterally into the deep marine deposits of the Aínsa slope complex (Cuisian-Lutetian deep marine deposits, fig. 3). In

140   the vicinities of the Mediano anticline, this unit includes cm-thick beds of wackestones and packstones interbedded with non-fossiliferous marls and reef limestones topped by siliciclastic and turbiditic intervals interbedded by platform limestones units containing large foraminifera. These sequences are overlain by the middle Lutetian Grustán Fm. (Garrido-Megías and Rios-Aragües, 1972) and the Entremón unit (Poblet et al., 1998) characterized by carbonate platform and reef limestones (Fig. 3). Limestones are found in the western limb of the Mediano anticline and grade basinwards into breccias.
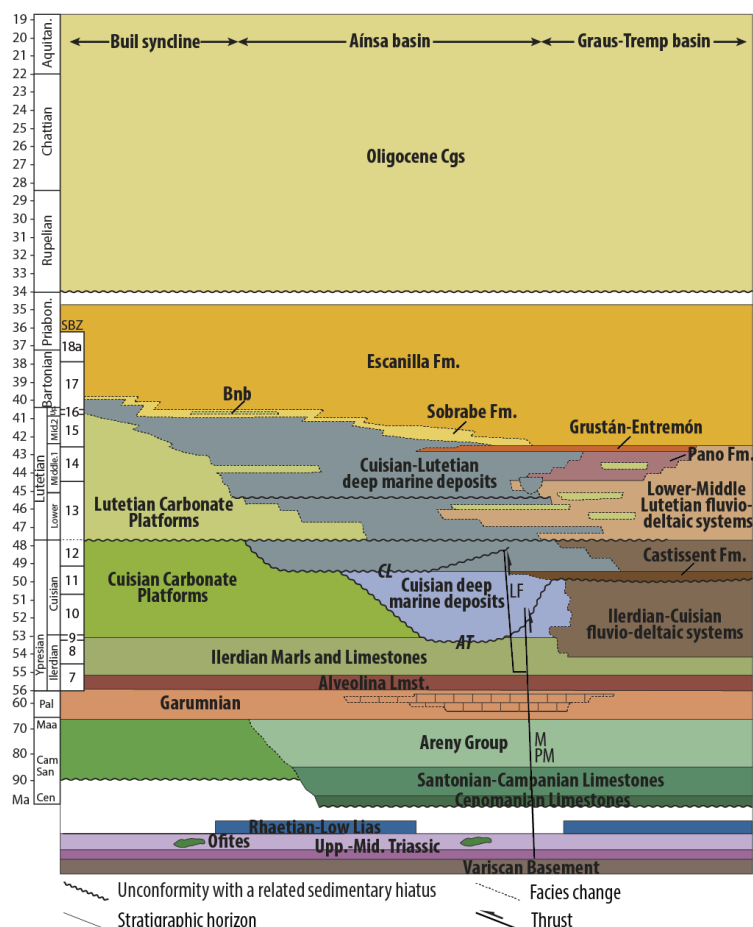
145

Figure 3. Chronostratigraphic diagram showing the main stratigraphic units of the Gavarnie-Sierras and Montsec thrust sheets. Diagram is designed to cover the area around Clamosa diapir and Mediano anticline. Bnb, Buil bummulitic bank; *AT*, Atiart unconformity; *CL*, Charo-Lascorz unconformity; M & PM, Montsec-Peña Montañesa thrust system; LF, La Fueba thrust system.

150   Middle-upper Lutetian fluvial red beds of the Escanilla Fm. grade from east to west into the deltaic sandstones of the Sobrarbe Fm. (De Federico, 1981), which in turn are the lateral equivalent of the upper part of the Aínsa slope complex deposits (Cuisian-Lutetian deep marine deposits, fig. 3). The youngest marine sediments correspond to the Buil Nummulitic bank (Mateu-Vicens et al., 2012). The Escanilla Fm. expands from Bartonian to Priabonian as a fluvial formation having scarce lacustrine limestones towards the lower part of the succession. Oligocene-Miocene continental sediments

155   unconformably lay over Escanilla Fm. and older units and extensively cover the southern half of the area.

Major unconformities have been recognized along the Aínsa Oblique Zone and have been used for establishing the chronology of the different structures in the area. North of the Clamosa diapir, the most significant and well-preserved unconformities are the early-middle Cuisian L'Atiart and the latest Cuisian Charo-Lascorz truncation surfaces (Figs. 3, 4)

160   (Soler-Sampere and Garrido, 1970; Mutti et al., 1988; Muñoz et al., 1994; Arbués and Corregidor, 1995). Flanking the Mediano anticline, an early Lutetian unconformity, namely the Mediano unconformity (Teixell and Barnolas 1995), extends along the anticline and truncates younger units to the north (e.g. Plaziat, 1984; Teixell and Barnolas) where it becomes concordant within the Lutetian deep marine deposits of the Aínsa slope complex. On top of it, Lutetian deposits exhibited a growth geometry involving some other internal unconformities that registered the kinematic evolution of the Mediano

165   anticline (Poblet et al., 1998). The Mediano unconformity has been extended to the south, around the Clamosa diapir (Teixell and Barnolas, 1995) as a single surface, however locally truncated by faults. New observations and biostratigraphic information point out that the nature of the unconformities is much more complex, as it is detailed in section 3.2 and the followings.

170   **3. The Clamosa diapir and Mediano anticline**

3.1 Biostratigraphic data

In order to establish a time constraint regarding the development of the Clamosa diapir and its relationship with the growth

175   of the Mediano anticline a bioestratigraphic analysis of large benthic foraminifera (LBF) was conducted. 4 paleontological sites with LBF were considered (location in Fig. 5). Sampling and procedures related to the biostratigraphic analysis and systematic criteria on the classification of LBF are detailed in the appendix A.

The samples contain LBF of a well-known age distribution. Site 1 (Sample ST-1) contains Assilina maior (Heim, 1908); A.

180   cuvillieri, (Schaub, 1981) and Nummulites campesinus (Schaub, 1966). These species are biomarkers of the Shallow Benthic Zone SBZ 12 according to Serra-Kiel et al., (1998). Site 2 (sample LP-1) contains N. manfredi (Schaub, 1966), a species corresponding also to the SBZ 12 (Serra-Kiel et al., 1998). On Site 3 (sample Cb-4) N. aff. boussaci, is found, a species

representative of the SBZ 13 biozone according to Serra-Kiel et al., 1998. On Site 4 (hand sample), a Idalina berthelini (Schlumberger, 1905) was described which yields to date the rock as Lutetian.

185

The chronostratigraphic correlation of the SBZ 12 and SBZ 13 has been calibrated, using magnetostratigraphic methods, by Rodríguez – Pintó et al. (2012, 2013 and 2022). Therefore, SBZ 12 is correlated with the boundary of chron C22n - C21r and the lower part of C21n, and thus, is located in the Ypresian – Lutetian transition. According to this correlation, Sites 1 and 2 can be dated between ~49 Ma and ~47 Ma (Gradstein et al., 2020). On site 3, a SBZ 13 biomarker is found, giving a younger

190 age. This biozone is early Lutetian and is calibrated as chron C21r to chron C20r (~47 Ma – 45.5 Ma, Gradstein et al., 2020).

SITE	SAMPLE	BIOMARKERS	SBZ biozones	Age	Age (Ma)
Site 1	**ST-1**	*Assilina maior, A. cuvillieri, Nummulites campesinus*	SBZ12	late Ypresian - early Lutetian	~49 - ~47
Site 2	**LP-1**	*N. manfredi*	SBZ12	late Ypresian - early Lutetian	~49 - ~47
Site 3	**Cb-4**	*N.* aff. *boussaci*	SBZ13	early Lutetian	~47– ~45.5
Site 4	**--**	*Idalina Berthelini*	SBZ13-16	Lutetian	~47– ~41.4

Table 1. Biostratigraphic sites, samples, biomarkers and biozones. Sites refer to those in Figure 5.

3.2. Surface geological structure

195 The Clamosa diapir features a triangle-shaped outcrop of Triassic evaporites, shales and carbonates (Fig. 4). It is bounded by outcrops (ranging from 0.5 to 2km wide) of different units, consisting of the Jurassic and Upper Cretaceous to Cuisian pre-growth sequences and the Lutetian to Oligocene syn- to post-folding-diapirism sequences. To the north of the Clamosa diapir, the main structural features include the Mediano anticline, the Bruis syncline, and the Tozal de Trillo homocline (Figs. 4 and 5).

200

The Mediano anticline is a detachment fold cored by up to 3 km of Triassic evaporites and shales, and extends north of the Clamosa diapir for about 20 km. In the southern sector, it trends N-S, displays an east vergence, and plunges about 10º to the north (Poblet et al., 1998), before bending to a NW-SE orientation and terminating beneath the turbidites of the Aínsa basin (Fig. 4). Northeast of the anticline, the La Fueba system consists of a SW-directed, NNW-SSE trending fold and thrust

205 system, which splays from the Montsec-Peña Montañesa thrust and mainly involves the Aínsa slope complex (Fig. 4).

A detailed examination of the southern termination of the Mediano anticline reveals that the north plunging crest line bends towards the NNE-SSW and becomes nearly horizontal, as proved by the map trace of the Santonian-Campanian to Campanian-Maastrichtian contact (Fig. 5, 6a). Folding dates from early Lutetian to Bartonian, as evidenced by syn-folding

210   growth strata (Barnolas et al., 1991, Holl and Anastasio, 1993, Teixell and Barnolas, 1995, Bentham and Burbank, 1996, Poblet et al., 1998). In both limbs, the early Lutetian to Bartonian syn-folding sequence depicts the superposition of two single progressive unconformities (Fig. 5), defining a composite progressive unconformity with an intermediate and localized angular unconformity within the growth sequence (Poblet et al., 1998).

215   In the eastern limb of the anticline, the Palo thrust brings the steeply dipping pre- and syn-folding sequences eastwards over the Bruis syncline (Fig. 5). The Bruis syncline is a gentle fold that trends N-S, plunges to the south, and involves a succession comprising the Cuisian turbidites to the Oligocene conglomerates. Coring the syncline, the Oligocene conglomerates unconformably overlies the Bartonian-Priabonian Escanilla Fm., which in turn truncates the middle-upper Lutetian Sobrarbe Fm. along the eastern limb of the syncline. A N-S, subvertical, west dipping, normal fault bounds the
220   Bruis syncline to the east. Further east, in its footwall, a WNW-ESE trending, 70° north-dipping, Upper-Cretaceous to Ilerdian sequence (i.e., the Tozal de Trillo homocline) is unconformably overlain by upper Cuisian turbidites. Notably, the Tozal de Trillo homocline succession is attributed to the Gavarnie-Sierras thrust sheet, as its Mesozoic to Cuisian succession resembles that of the Mediano anticline.

225   The boundary between the Mediano anticline and the Clamosa diapir is marked by a diapiric, structural contact that connects to the south and west with the N010E-oriented, east-dipping Ligüerre normal fault (Fig. 5). The footwall of this fault involves Lutetian to Priabonian units unconformably overlying Upper Cretaceous carbonates and Paleocene rocks to the north, close to the Samitier Castle. Its hanging wall includes the Lutetian to Priabonian Escanilla Fm., either overlaying or truncated by Triassic rocks of the Clamosa diapir.
230   The boundary between the Clamosa diapir and the Oligocene conglomerates of the Bruis syncline stands as a 60° north-dipping normal fault, whose lateral continuation is challenging to trace, leaving open the possibility that the conglomerates also directly overlie Triassic rocks (Fig. 5). Further east, south of the Tozal de Trillo homocline, along the northeastern limit of the Clamosa diapir, Triassic rocks cropping out along a W-E, 500 m wide stripe are unconformably overlain by upper Cuisian-lower Lutetian marls (as dated after foraminifera content, Site 1, Fig.5, see appendix A).

235

In the eastern flank of the Clamosa diapir, the fluvial sediments of the Escanilla Fm. and the Oligocene conglomerates are truncated by a system of west-dipping curved or wavy NNE-SSW normal faults (Fig. 5, 6c). Its footwall predominantly consists of Upper Cretaceous units unconformably overlain by lower to middle Lutetian deltaic and carbonate units. There, the Upper Cretaceous succession is usually capped by a meter-thick breccia of Upper Cretaceous-derived rocks that rapidly
240   grades upwards into lower Lutetian rocks. In the hanging wall of this fault system, the Oligocene conglomerates unconformably overlie the Escanilla Fm. and the Triassic evaporites. To the southeast of the Clamosa diapir, the Lutetian succession becomes nearly horizontal and is gently truncated by the Escanilla Fm. and the Oligocene conglomerates to the south.
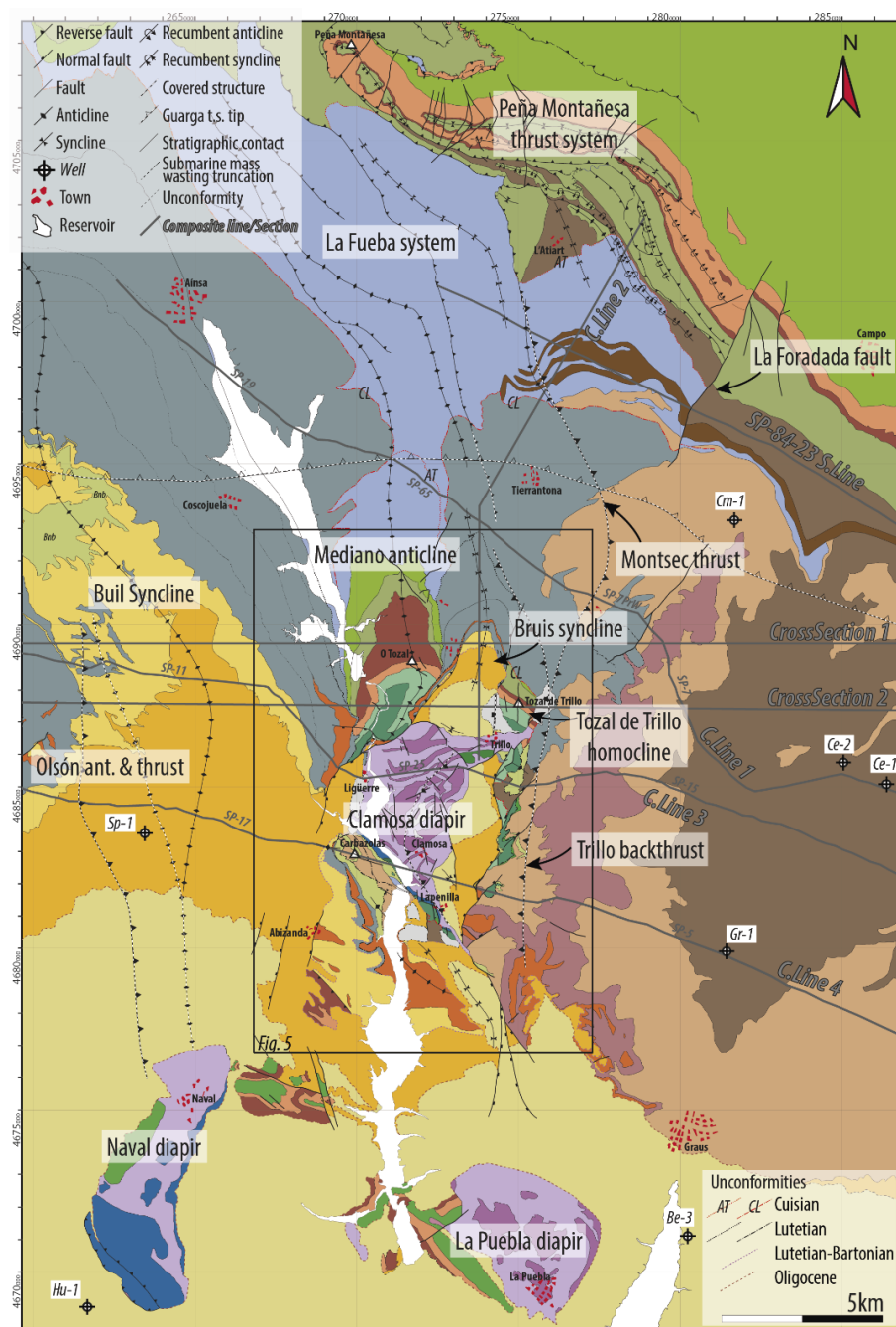
Figure 4. Geological map of the area studied. See figure 3 for the colour legend of stratigraphic units. Main structural features described in the text are labelled. Dark grey lines represent seismic sections, composite lines and cross-sections traces. Note that black-white dashed lines denote buried structural features. The tip line of the Guarga basement thrust sheet is represented as a dashed black and white line with open black arrows. Southern and northern areas are adapted from Barnolas et al. (1994a,b; 1999) and Santolaria et al. (2014).

250
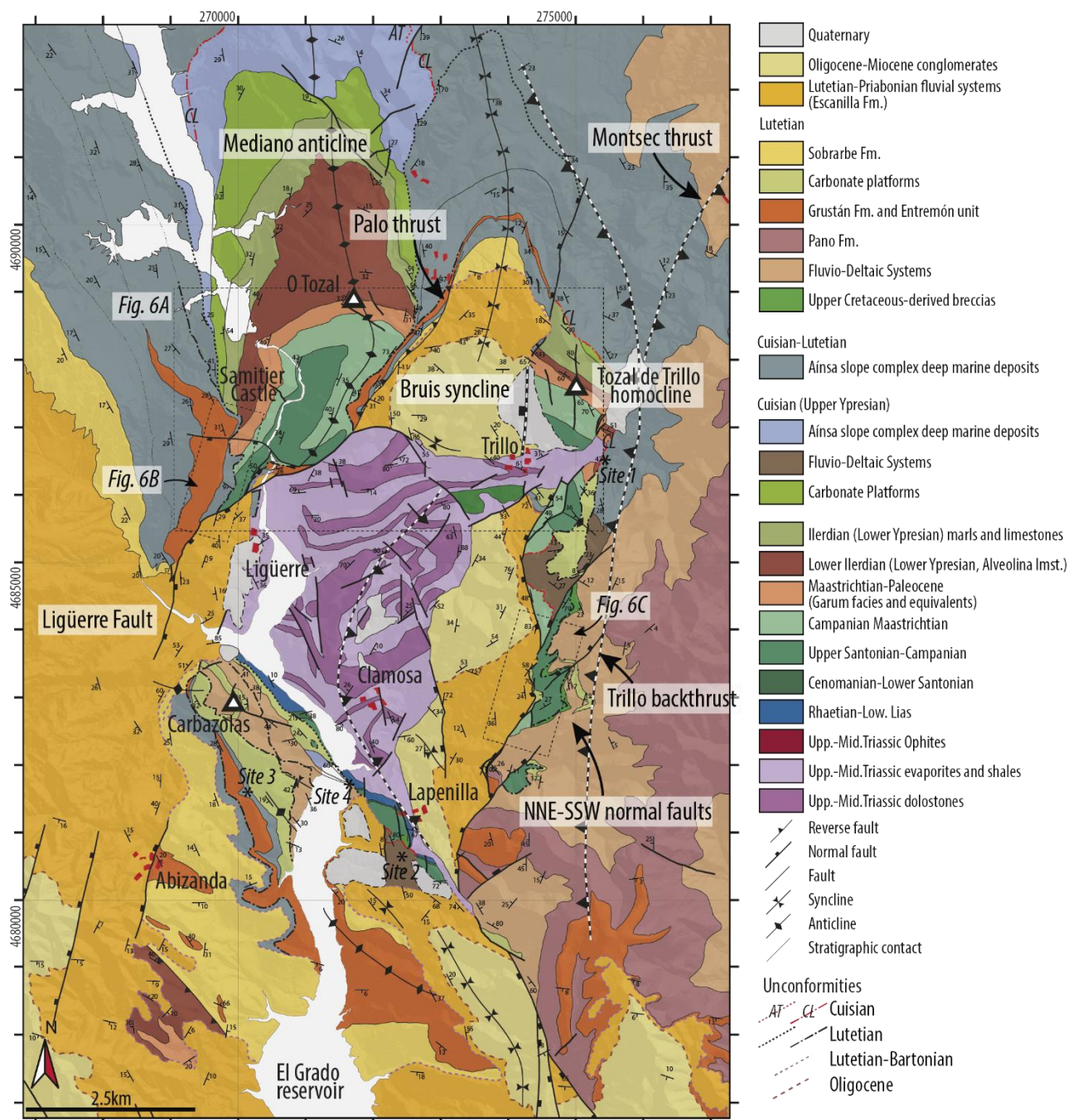
Figure 5. Geological map of the Mediano anticline-Clamosa diapir area showing the structural features described in the text and paleontological sites included in the biostratigraphic analysis shown in the appendix A. Partly adapted from Barnolas et al. (1994b).
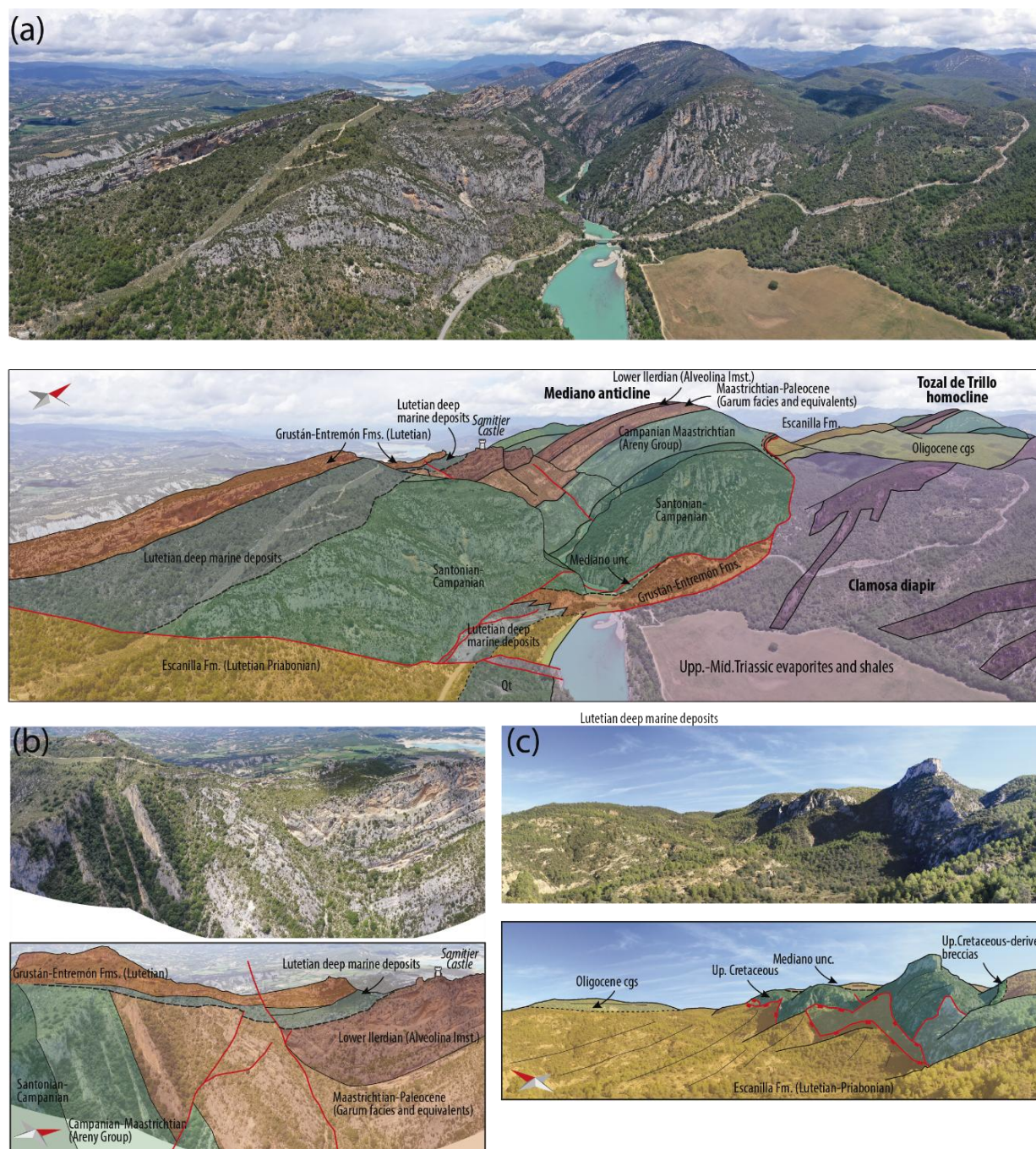
Figure 6. (a), Drone image of the northern boundary of the Clamosa diapir and the Mediano anticline and its interpretation. (b), Close up view of northwestern flank of the Clamosa diapir and Mediano anticline. (c), Interpreted picture of the NNE-SSW trending, west-dipping extensional faults related to the collapse of the diapir during Oligocene. See their location in Fig. 5.

In the southwestern flank of the Clamosa diapir, there is a 5.5 km long, NW-SE oriented, outcrop of folded and faulted Jurassic dolostones and Upper Cretaceous limestones and sandstones (Fig. 5). In the Carbazolas sector, the Mesozoic

260   sequence is overlain by Lutetian carbonates, followed by Lutetian fluvio-deltaic units, carbonates and turbidites, generally trending NW-SE. This sequence features several internal unconformities, which may resemble or be equivalent to those found along the limbs of the Mediano anticline. This sequence is also unconformably overlain by the middle-upper Lutetian Sobrarbe Fm. and by the Lutetian-Priabonian Escanilla Fm. To the southeast, near Lapenilla village, Triassic evaporites extend for 2.5 km along a narrow band, trending NW-SE. There, upper Cuisian to lower Lutetian fluvio-deltaic rocks (as

265   dated after foraminifera content, Site 2, Fig.5, see appendix A), unconformably overlie the Triassic to Upper Cretaceous succession. This stripe of Triassic evaporites links to a set of NNW-SSE to N-S faults that die out into the Oligocene conglomerates to the south (Fig. 5). To the west of the Mediano anticline and the Clamosa diapir, the most prominent structure at surface is the gently south-plunging Buil syncline (Fig. 4). The southern part of the area is extensively covered by Oligocene conglomerates, except for localized outcrops of folded and faulted Upper Cretaceous to Ilerdian rocks and

270   Triassic evaporites coring elongated to rounded diapirs (Naval and La Puebla respectively) (Figs. 2, 4).

3.3. Seismic interpretation and subsurface structure

To illustrate the subsurface structure of the studied area, 12 seismic lines and 2 key cross-sections are used (see Fig. 4 for

275   location and Figs. 7 and 8 for their interpretation). These seismic lines and cross-sections are strategically located: to the north, along the Aínsa basin (SP-84-23); across the Mediano anticline and the Montsec thrust sheet front (Composite Line 1, including the seismic profiles SP-19, SP-65, SP-7PrW and SP-7 and Cross Sections 1 and 2; see Fig. 7); across the La Fueba system and along the Bruis syncline (Composite Line 2, including seismic profile SP-84-19); and across the Clamosa diapir (Composite Lines 3 and 4 including the seismic profiles SP11, SP25, SP15, SP-17 and SP-5; see Fig. 8). The traces of deep-

280   seated and buried structures derived from seismic interpretations and the construction cross-sections are represented in Fig. 4 as black and white dashed lines, aiding the description of the subsurface structure.

3.3.1. The Montsec-Peña Montañesa thrust sheet

285   In the north of the study area, the Peña Montaseña thrust system links with the L'Atiart thrust, to the south and continues at depth with the Montsec thrust (SP-84-23 line, Figs. 4 and 7). The Montsec thrust sheet involves a Jurassic-Upper Cretaceous to Ilerdian succession, slightly truncated by the La Foradada tear fault and, further west, the thrust branches off into several thrusts belonging to the La Fueba System. Along Composite Line 1, the Montsec thrust sheet shows a similar geometry as in SP-84-23, but the La Fueba system and La Foradada fault are absent as they do not extend that far south (Fig. 4). To the

290   south, the Montsec thrust acquires a NNE-SSW orientation and is truncated at depth by the Trillo backthrust (see Fig. 4 and Cross Sections 1 and 2 and Composite Lines 3 and 4, Figs. 7 and 8). The cross-sections generally show the Montsec-Peña

Montañesa thrust sheet as a gently folded Triassic to Ilerdian succession, with nearly parallel seismic reflectors that thin towards the west and south (e.g. Soto et al., 2002; Fernández et al., 2012). In contrast, Cuisian – Lutetian sediments show tens of kilometres wide growth strata geometries, generally thickening towards the west (see Composite line 1; Fig. 7). The

295 truncation of the Montsec thrust sheet by the Trillo backthrust suggests that the frontal tip of the Montsec thrust was truncated, uplifted, exhumed and eroded (see section 5 for further discussions).

3.3.2 The Gavarnie-Sierras thrust sheet

300 The Gavarnie-Sierras thrust sheet in the footwall of the Montsec-Peña Montañesa thrust sheet features a laterally variable geometry. Conversely to the Montsec-Peña Montañesa, the Gavarnie-Sierras thrust sheet shows a shorter structural wavelength, localized growth strata geometries hundreds-of-meters-wide, and a markedly thinner Triassic to Ilerdian succession that maintains the western and southern thinning trends.

305 To the north of the study area, in the footwall of the Montsec thrust, the Gavarnie-Sierras thrust sheet is distinctly imaged as a nearly parallel sequence detached over the Guarga basement thrust sheet, which in turn thrust over the Ebro basin foreland units (SP-84-23 and Composite Line 1, Fig. 7). In map view, the Guarga thrust has a curved shape with an overall N100W orientation, i.e. highly oblique to cover structures (Fig. 4). Along Composite Line 1 (Fig. 7) the Mediano anticline is imaged as an asymmetric, east-verging, open anticline, with its eastern limb truncated by a thrust.

310

To the south, the Mediano Anticline tightens and increases in amplitude. In cross-section 1 (Fig. 7), it features a wavelength of about 8 km and an amplitude of 3.6 km. The anticline appears as a slightly asymmetric detachment fold cored by a large accumulation of Triassic evaporites, with its western and eastern limbs dipping 40 to 70-80 degrees to the west and east, respectively. Its western flank abuts the South Pyrenean sole thrust, but its eastern flank does not; it occupies a higher

315 structural position below the Bruis syncline (Fig. 7, cross-section 1). Further south, along cross-section 2, the eastern flank of the Mediano anticline reduces to a thousand-meter-wide panel of Upper Cretaceous, with the Bruis syncline directly overlying Triassic evaporites. Composite Line 2 (Fig. 8) better illustrates the north to south shallowing of the Mediano anticline eastern limb, note this composite line run nearly parallel to it (Fig. 4). In the northern part of this composite line, the Montsec thrust and the La Fueba system thrust over a seismically well-imaged Upper Cretaceous-Lower Eocene sequence of

320 the Gavarnie-Sierras thrust sheet. Both the Montsec-Peña Montañesa and Gavarnie-Sierras thrust sheets are tilted by the Guarga basement thrust sheet, with the tip point located halfway along the section. Seismic interpretation reveals that there is little to no Triassic evaporites between the Gavarnie-Sierras and the Guarga basement. Yet, they are decoupled. South of the tip point, the Gavarnie-Sierras sequence progressively acquires a north-dipping inclination as it approaches the Clamosa diapir (Fig. 8). Unconformably atop the Gavarnie-Sierras sequence, the Lutetian slope deposits of the Bruis syncline gently

325 dip southward, towards the Clamosa diapir. And, unconformably on top of them, the Escanilla Fm. and the Oligocene

conglomerates define a restricted trough towards the Clamosa diapir (Fig. 8, note that this section runs parallel to the axis of the Bruis syncline).

Back to the W-E cross-sections (Fig. 7), a west dipping normal fault separates the Lutetian to Oligocene rocks of the Bruis
330 syncline from the Tozal de Salinas homocline, which thrust over the Peña Montañesa-Montsec thrust sheet succession (see Trillo backthrust in Fig. 7, cross-sections 1 and 2). A triangular piece of the Gavarnie-Sierras units remains in the footwall of the Montsec thrust and the Trillo backthrust.

Along the Clamosa diapir transects, in the western limb of the Mediano anticline, the pre-folding succession dips
335 approximately 40-50 degrees to the west, while near the Clamosa diapir, it becomes nearly vertical (SP-25, Composite line 3, Fig. 8) or is folded and overturned (Composite line 4, Fig. 8). Along the western flank of the diapir, Lutetian growth strata lie moderately to gently dipping in SP-11 (Composite line 3, Fig. 8) but are folded and faulted in Composite Line 4 (Fig. 8). The top of the Clamosa diapir is bounded by a set of diapir-converging faults that involve limited Upper Cretaceous rocks but mostly Lutetian to Oligocene units, which are suggested to lie directly on top of Triassic evaporites (Fig. 8). The eastern
340 boundary of the diapir is represented by the Trillo backthrust that brings the Upper Cretaceous units to the surface (Fig. 5 and Fig. 8) and truncates the Montsec thrust (as in previous sections).

To the west of the Clamosa diapir and Mediano anticline, the Buil syncline appears as an open syncline. Beneath it, subsurface data reveal the existence of the Olsón anticline, a thrust-related anticline fossilized by Lutetian deposits. In map view, the Olsón anticline trends N-S to N150E for approximately 11 km (Fig. 4) and links with the Naval diapir.

345
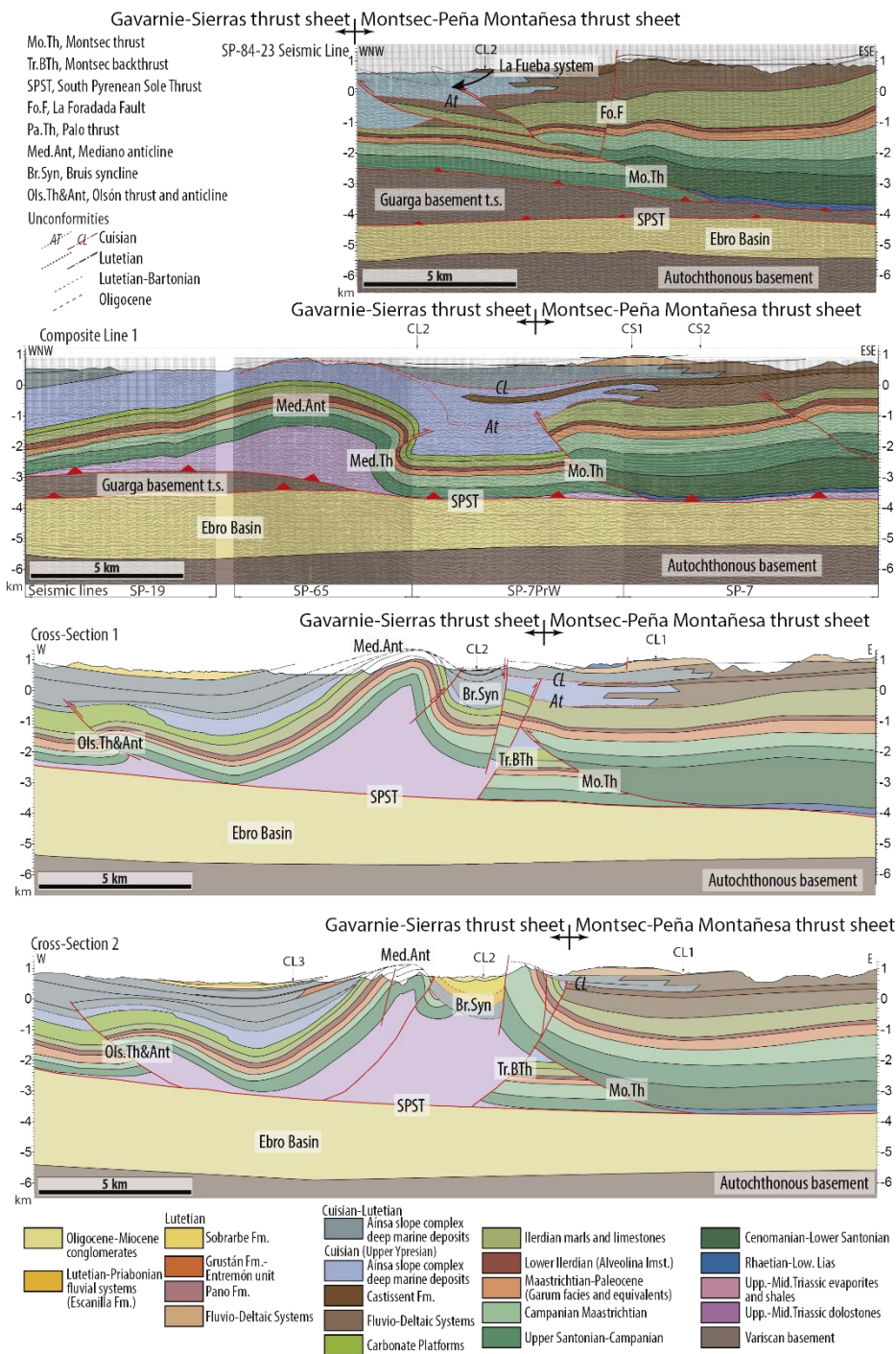
Figure 7. Cross sections and interpreted seismic lines illustrating the subsurface structure of the Montsec-La Fueba system (SP-84-23 seismic line), and the north to south along strike variability of the Montsec-Mediano anticline structures (Composite line 1, Cross-section 1 and Cross section 2). See fig. 4 for location.

350
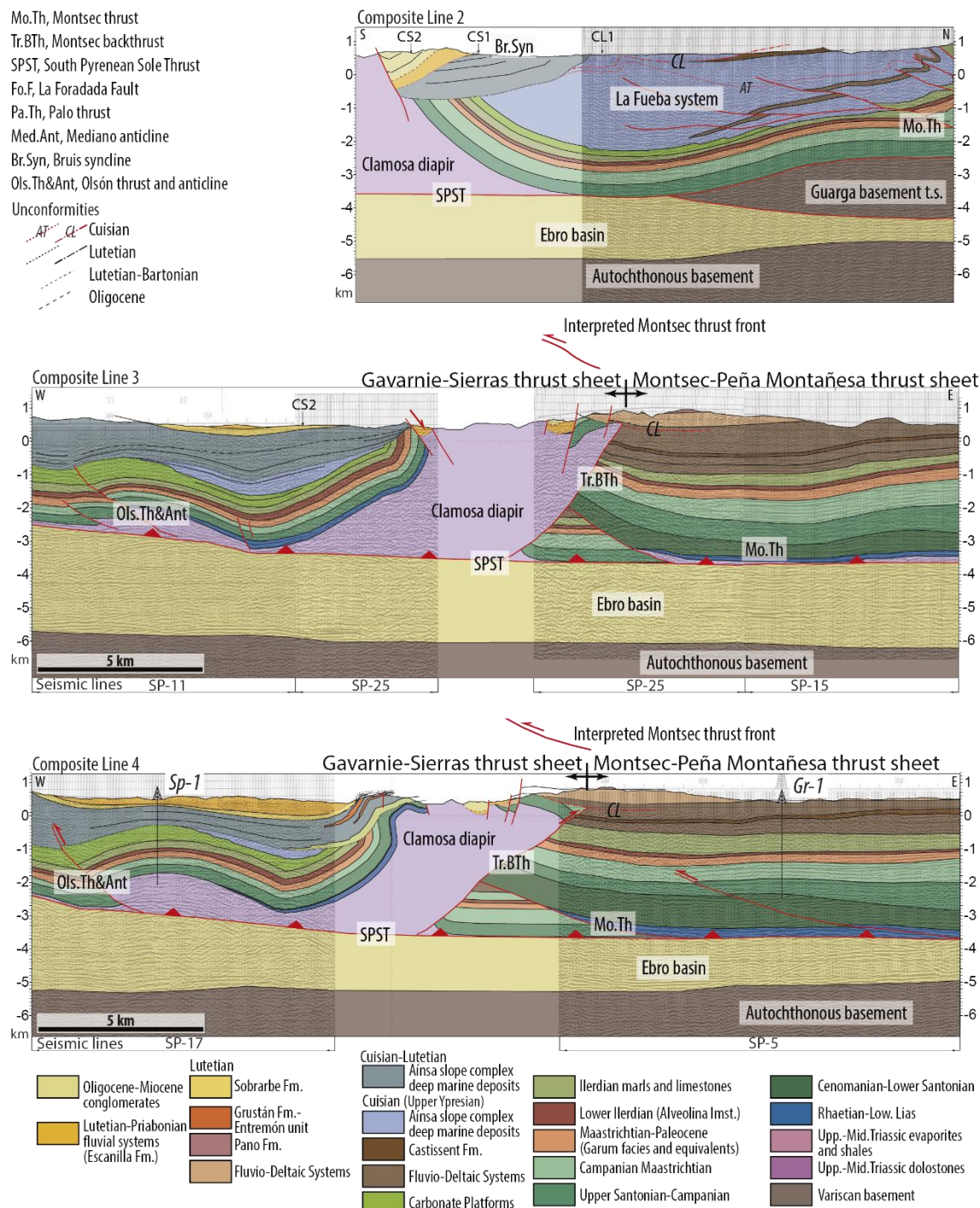
Figure 8. Interpreted Composite lines 2, 3 and 3 illustrate the subsurface structure of the Montsec-Clamosa diapir system. See fig. 4 for location. Sp-1: Surpirenaica-1 well.

4. Structural evolution of the Clamosa diapir and Mediano anticline in the western South Pyrenean Central Salient

355

This section aims to frame the formation of the Clamosa diapir and the Mediano anticline within the structural and kinematic evolution of the western half of the South Pyrenean Central Salient, and contextualize the formation and evolution of salt diapirs in contractional settings. As introduced earlier, this area of the Pyrenees is characterized by along strike structural changes and N-S trending structures that underwent up to 80º of syn-orogenic vertical axis clockwise rotation (Mochales et

360 al., 2012; Muñoz et al., 2013). In this context, we propose that the Clamosa diapir is a purely contractional diapir whose salt accumulation is inherited from a Triassic extensional basin that incorporated into the fold-and-thrust belt system together with the formation of the Trillo backthrust and the Mediano anticline. So, we interpret the formation of the Clamosa diapir as a combination of salt inflation, folding and thrusting, followed by piercing of the cover triggered by erosion and longitudinal stretching upon vertical axis rotation. Finally, the diapir underwent extensional collapse. In the following, we provide a

365 detailed and justified evolutionary model for the Clamosa diapir, the Mediano anticline and La Fueba thrust system. The proposed evolution is illustrated and discussed through schematic sections (Fig. 9) and a plan view restoration (Fig. 10).

The Clamosa diapir belongs to a salt tectonics province in the Gavarnie-Sierras thrust sheet, characterized by thick Middle-Upper Triassic evaporites, mudstones and carbonates. In this province, diapirs have pierced the Upper Cretaceous to

370 Miocene succession and have been fed from a thick salt layer as revealed by geological surface and subsurface data, and gravity data (Fig. 4, Santolaria et al., 2016, 2024). A key point in the study area is the original distribution and thickness of the Triassic evaporites and the timing of interpreted salt inflation events. Burrel and Teixell (2021) postulated a thick and continuous Triassic evaporitic basin, over a faulted basement, thickening northwards from 1km in the southern Gavarnie-Sierras thrust sheet to 3km beneath the Montsec thrust sheet. These authors suggest that accommodation space of Jurassic to

375 Upper Cretaceous basins resulted from downbuilding and the surrounding salt walls fed by salt flow in multiple directions (Burrel and Teixell, 2021). They suggested that downbuilding coexisted with shortening since Palaeocene, and the salts walls were subsequently squeezed during the Paleogene. On the other hand, Santolaria et al. (2016) suggested that the salt in the Gavarnie-Sierras thrust sheet was inflated by salt flow evacuated from beneath the Montsec thrust sheet as it was transported to the south. Conversely, Hudec et al. (2021) proposed that the salt province of the Gavarnie-Sierras thrust sheet

380 developed in an isolated southern Triassic graben and that salt flowed northward from Jurassic to Upper Cretaceous times. Salt would have been inflated against the structural high bounding the basin northwards that would coincide with the Montsec thrust sheet and the Graus-Tremp piggy-back basin. The Montsec thrust would correspond to a salt wall developed since late Jurassic, with its western tip corresponding top the Clamosa diapir (Hudec et al., 2021). To tackle the question of the pre-shortening distribution of Triassic evaporites, we focused on the distribution of some distinct Mesozoic units around

385 the Clamosa diapir, mainly the lower Jurassic carbonates and the postrift upper Cenomanian limestones (Fig. 3). The Triassic evaporites were deposited during the last stages of the first rifting event that affected Iberia during the break-up of Pangea

(López-Gómez et al., 2019). Above, the Hettangian carbonates represent either the last stages of rifting or the start of the sag phase. Triassic basins have been completely inverted and deformed during Pyrenean deformation, yet some of them can be reconstructed (López-Gómez et al., 2019). In the Clamosa diapir, the presence of the lower Jurassic carbonates at its

390   southern margin suggests the existence of an upper Triassic depocenter, in contraposition of the northern margin of the diapir where the Upper Cretaceous sediments rest directly above the Keuper, pointing out to the existence of a structural high (Fig. 9a, b). Interestingly, a 20-30 meters-thick Upper Cenomanian sequence is also preserved in what it was the southern basin, and which is nowadays the southwestern limb of the Clamosa diapir (Fig.5). This sequence developed northwards in the Montsec thrust sheet above the Upper Triassic evaporites and a thicker and more complete Jurassic succession, on what it

395   was the proximal domain of the North Iberian Early Cretaceous rifted margin. Hettangian carbonates are also observed around the diapirs of the salt tectonics domain extending south of the Clamosa diapir. Thus, in the central part of the study area a southern salt basin would be separated from a northern basin by a structural high, aligning with the interpretation by Hudec et al. (2021). However, from our observations, this high is located south of the Montsec thrust and would have controlled the location of the Montsec thrust as well as the Trillo backthrust. Moreover, the southern basin, would be oblique

400   to the northern one and terminates to the west. It would be most probably connected with the northern salt basin eastward, as suggested by the deposition of the upper Cenomanian limestones. In any case, the observed salt structures, as well as thrusts and related folds would have been controlled by the pre-shortening 3d configuration of the Triassic basins and highs.

The absence of any middle Jurassic to Upper Cretaceous stratigraphic record in the western Sierras Marginales, including the

405   salt province above referred, do not support the idea of salt flow during this time, and consequently the formation of salt structures, as suggested by Hudec et al., 2021 and Burrel and Teixell, (2021). The Santonian to Paleocene succession formed a south and west-thinning sedimentary wedge above the southern Triassic basin, as well as atop of the structural high and the Peña Montañesa-Montsec thrust sheet (Fig. 9b). There is no evidence of local thickness changes of this succession, discarding any local salt movement in this area during Late Cretaceous to late Cuisian (Fig. 9b), contrary to what is observed

410   eastward in the Gavarnie-Sierras thrust sheet (Ramirez-Perez et al., 2024). Deposition of this Upper Cretaceous to Paleocene succession occurs at the same time as the Cotiella-Bóixols thrust sheet and related basement thrust sheets were already emplaced north of the studied area (Fig. 10b).

Later, between Paleocene and Cuisian, the Montsec thrust emplaced as a SSW-directed thrust (Fig. 10c) coevally to the

415   sedimentation of fluvio-deltaic and deep marine sequences along the Tremp-Graus and Aínsa basin slope complex, respectively. The Montsec thrust likely nucleated at the southern pinch-out of the northern salt basin (note that pinch-out does not necessarily refer to the disappearance of Triassic evaporites but to a significant thinning of them that may represent a mechanical discontinuity in the salt décollement) (Fig. 9c).
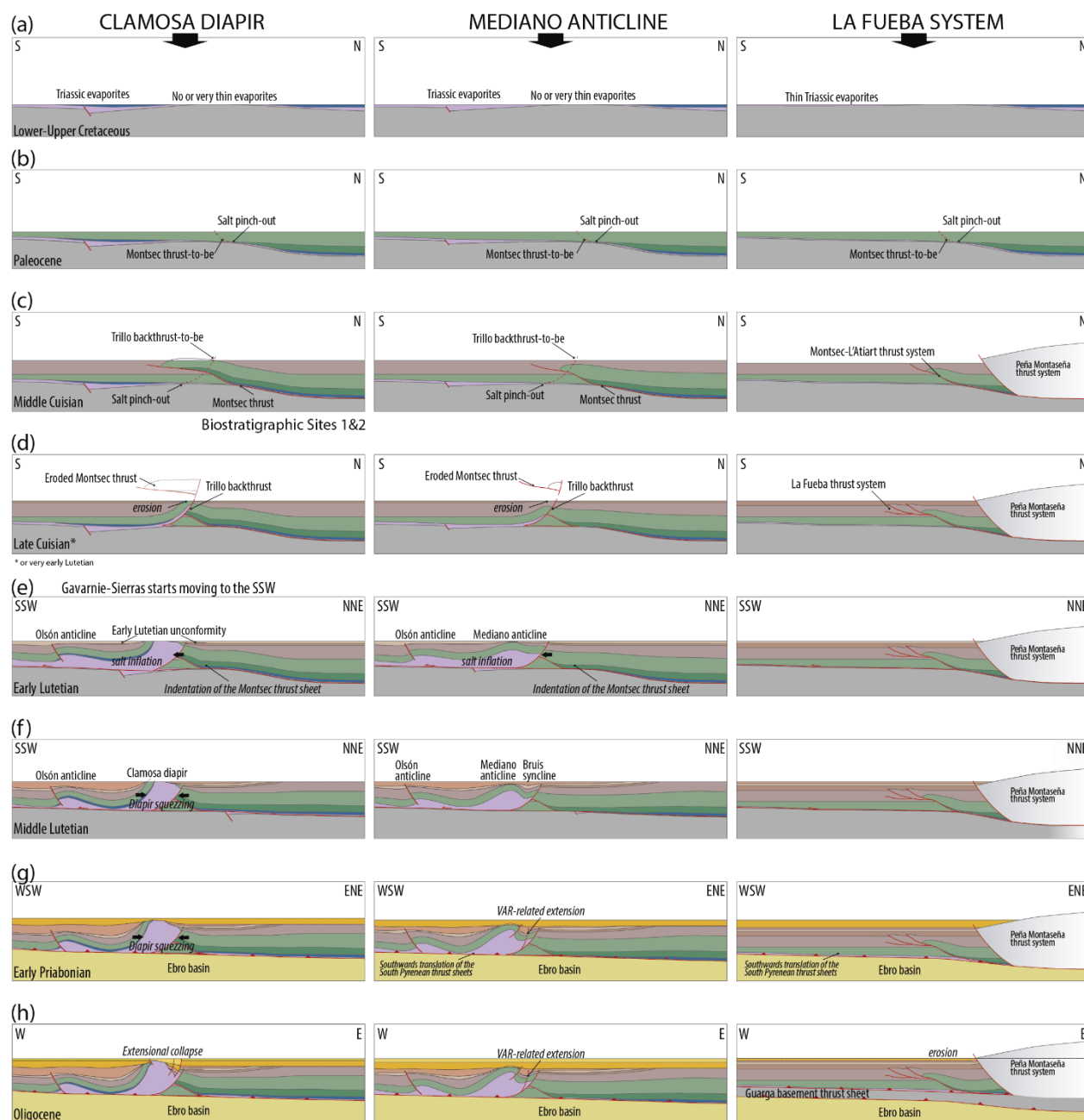
Figure 9. Stepped reconstruction that illustrates the along strike differences of the formation of Clamosa diapir (left column), the Mediano anticline (central column) and the Peña Montañesa-La Fueba system (right column). Sketches gather representative surface and subsurface geological information; they are not structural restorations. Obliqueness, out-of-plane deformation and vertical axis rotation prevent any reliable cross-section restoration. Yet, some of the ideas illustrated here come from local and punctual restorations. Note the change in the orientation of the sketches. Such changes account for the Middle to Late Eocene vertical axis rotation. An approximate location of the section is shown in the plan view reconstruction of Fig. 10.
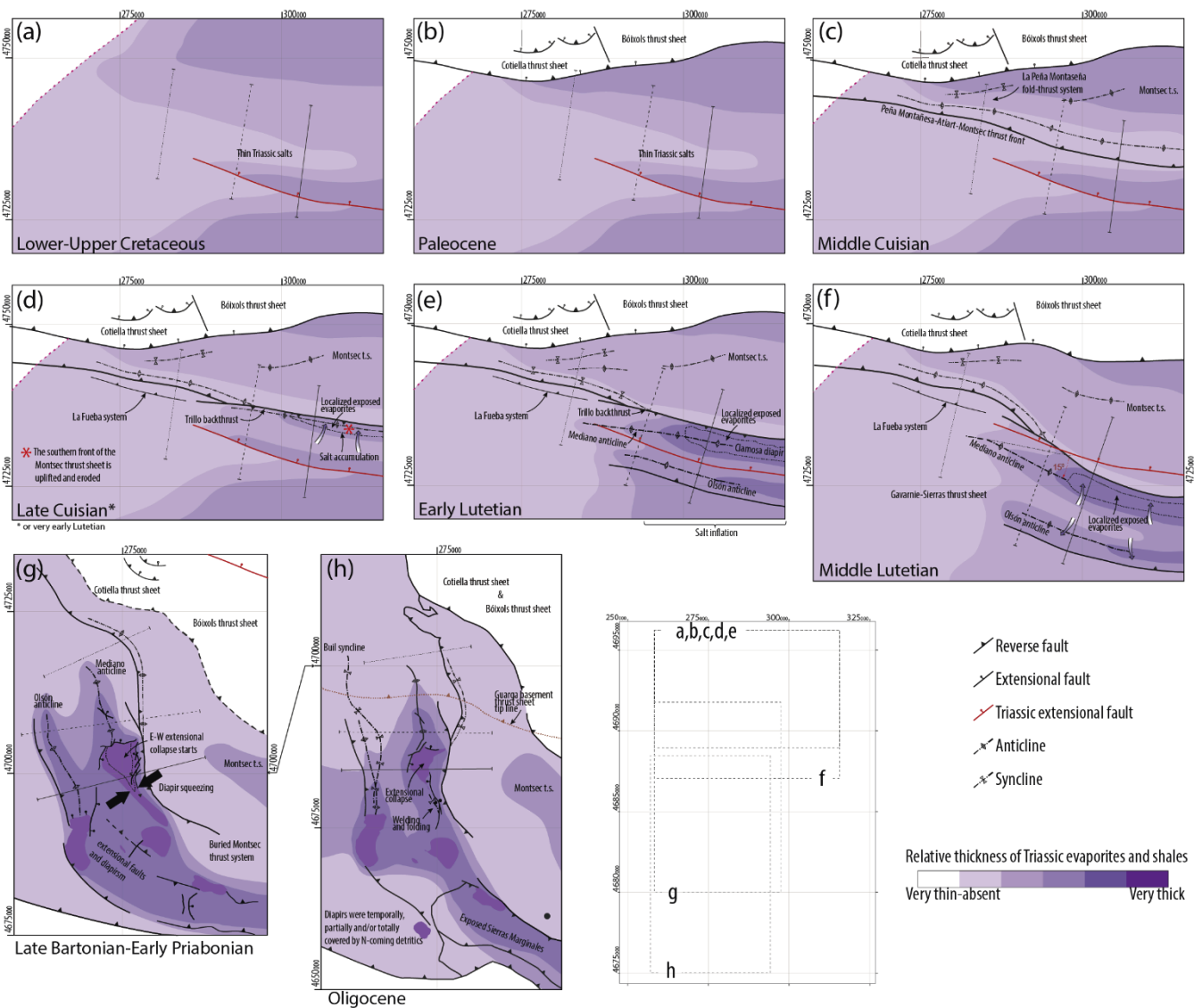
Figure 10. Plan view reconstruction of the studied area (partly modified from Muñoz et al., 2013 and Santolaria et al., 2014). Weak to strong purple denote thin to thick Triassic salt accumulations. Red line represents the basement normal fault bounding the southern salt basin as seen in Fig. 9.

Following the emplacement of the Peña Montañesa-L'Atiart-Montsec thrust system, contractional deformation was transmitted to the southern salt basin and the Trillo backthrust formed (Fig. 9d) as one of the earliest structures related to the deformation of the Gavarnie Sierras thrust sheet. Emplacement of the Trillo backthrust has been dated after foraminifera

content. Emplacement postdates the Montsec-Peña Montañesa thrust sheet, since the Trillo backthrusts truncates it, and predates deposition of SBZ12 sediments (see section 3.1, Table 1) found in Salinas de Trillo (Site 1) and Lapenilla (Site 2) villages; these SBZ12 sediments overlay Triassic evaporites and shales (Figs. 7 and 8). This backthrust formed as WNW-
440   ESE structure along the northern edge of the southern salt basin, synchronously with the La Fueba system westward the edge of the southern salt basin (Fig. 10d). Its emplacement involves the truncation of the Montsec thrust whose southern termination was brought upwards, exposed and eroded together with the Gavarnie-Sierras succession. Structural uplift was significant enough to bring up the Triassic evaporites to the surface, as observed and dated in the NE and SE corner of the Clamosa diapir (see biostratigraphic Sites 1 and 2, Fig. 5 and appendix A) where upper Cuisian to earlier Lutetian deposits
445   unconformably overlies Triassic evaporites and shales.

Coeval to the emplacement of the Trillo backthrust, salt inflation took place along the southern salt basin (Fig. 9e, 10e, the nature of inflation is discussed in the following section). Inflation was maximum in the vicinity of the Clamosa diapir and south of it and progressively attenuated to the WNW to finally disappear towards the pinch-out of the Triassic evaporites and shales (Fig. 10e). During the squeezing of the southern salt basin, the Mediano and Olsón anticlines grew (Fig. 9e, 10e). The
450   Mediano anticline registered a peak of uplift during early to middle Lutetian as shown by the stratigraphic record, subsequently decelerating during middle to late Lutetian (Poblet et al., 1998). At that time, the Olsón and specially the Mediano anticline tightened while the syncline in between both deepened into salt (Fig. 9f). Anticline growth occurred synchronous to their vertical axis rotation (Muñoz et al., 2013) while the Clamosa diapir was being squeezed (Fig. 9f, 10f).

During Bartonian-Priabonian times, folding of the Mediano anticline slowed down and halted. At that time the fluvial
455   deposits of the Escanilla Fm. deposited extensively over the area (Fig. 9g). The Escanilla Fm. lies directly on top of Triassic evaporites and shales of the Clamosa diapir suggesting a continuous surficial extrusion of Triassic at that time. This took place synchronously to the southward translation of the Pyrenean thrust sheets that thrust over the Ebro foreland basin deposits (Fig. 9g, 10g). During this event, differential displacement triggered a second phase of clockwise vertical axis rotation that lasted from Priabonian to Chattian (Muñoz et al., 2013). Differential displacement was partially favoured by the
460   differential closure of the Clamosa diapir, which resulted in welding of the diapir's southern edge (Fig. 10h) and crestal collapse to the north (Fig. 9h). The late Eocene to Oligocene diapir collapse is evidenced by i) N-S extensional faulting into the diapir in the eastern and western flanks where the Escanilla Fm. and Oligocene conglomerates are deposited on the hanging wall of these faults and ii) north-directed normal faulting of the Bruis syncline where the Escanilla Fm. and Oligocene conglomerates filled a localized depocenter north of Trillo town.

465

5. Discussion

Despite diapirism is less common in contractional settings than in extensional ones (i.e., Vendeville and Jackson, 1992; Jackson and Vendeville, 1994) it is also a remarkable feature in many fold-and-thrust belts. Those that incorporate and
470   deform pre-shortening early salt structures in rift to rifted margins settings (e.g., Granado et al. 2021, 2023; Santolaria et al.

2021; 2022) usually display a larger budget of salt and salt-related features, such as the Fars province of the Iranian Zagros (Jahjani et al. 2009; Snidero et al. 2020) or the Persian Gulf (Perotti et al. 2016; Snidero et al. 2020), the Northern Calcareous Alps of Austria (Granado et al. 2019; Strauss et al. 2023; Fernández et al. 2024) or the Betic Cordillera of Spain (Escosa et al., 2018; Flinch and Soto, 2022; Canova et al., 2025).

475

Salt is easily mobilized upon contraction. Due to its viscous behaviour, shortening of salt horizons entail their immediate redistribution by generalised thickening. Yet, diapirism in contractional systems with no inherited salt structures is commonly hampered by several factors, fundamentally the strengthening of the sedimentary overburden by thickening, either by means of thrust stacking, syn-contractional sedimentation or both. However, salt inflation, overburden piercing and salt extrusion to the syn-orogenic surface can happen when a series of factors coalesce. So, diapir-favouring processes in fold-and-thrust belts include: a thin and weak sedimentary overburden, either pre-existent, or developed by other means, such as by erosion, faulting, restricted sedimentation on top of inflated salt bodies, or combinations of these. Erosion and faulting of thrust wedges and related folds can happen by emergent thrusting and thrust stacking, amplification of detachment folds and formation of fold-accommodation faults (e.g., Coward and Stewart, 1995; Sans and Koyi, 2001; Santolaria et al. 2015; Mitra, 2002; Rowan, 2020). A mobile salt detachment thicker than its sedimentary overburden will strongly favour diapir-formation as well, particularly in combination with the above-mentioned elements. Some of these factors coalesce in the Clamosa diapir, being inflation of the Triassic evaporitic horizon during early Lutetian one of the keystone ones. Salt inflation is inferred after the structural uplift of the Jurassic to early Cuisian succession observed in the Gavarnie-Sierras thrust sheet as registered by the basal Lutetian unconformity (Fig. 9E). Such uplift mainly resulted from shortening of the southern Triassic basin. It can be argued that salt might come from the east, but this was also an area of inflation at that time; or from the west as proposed by Holl and Anastasio (1993), but there is no evidence of salt withdrawal structures or growth strata currently north of the Clamosa diapir (west in Lutetian times); or from the north, from the Montsec thrust sheet as proposed by Santolaria et al. (2016), since there was no across-strike connection of the northern and the southern Triassic basins. So, we propose that salt inflation resulted from the thickening of the Triassic salts of the southern Triassic basin due to the displacement of the Montsec thrust front to the SSW. The Montsec thrust front acted as a buttress that embedded into salt while preventing it to migrate northwards.

Balance between favourable and unfavourable factors during mountain building is sensitive to subtle changes that may enhance or halt the formation of diapirs. In their seminal work, Sans and Koyi (2001) propose erosion of anticlines rising to the top free surface increases differential loading on the underlying décollement salt layer and thins and weakens their overburden, promoting diapirism without any change in the dominant contractional tectonic regime. In a simplistic 2d approach of a contractional system, detachment anticlines increase the cross-sectional area during the early stages of development (i.e., Poblet et al., 1998) to allow salt flow towards their cores, while erosion has to be sufficiently deep-reaching for salt to pierce its overburden. As shown for an Appalachians case by Wiltschko and Chapple (1977), open

505   detachment folds with interlimb angles >70° allow salt to accumulate in their cores, whereas fold tightening conversely will promote backflow into the underlying source layer. Since detachment folds need syn-contractional sedimentation to amplify and grow (Poblet et al. 1998), the synclinal troughs adjacent to growing anticlines are depositional sites that sink below the regional level by evacuating salt from the underlying décollement (Mitra, 2003). In the crestal area the salt/overburden thickness ratio is greater than both the initial ratio and that under the synclinal troughs. Sedimentation rate must be lower

510   than uplift rate for the growing detachment anticline to keep the hinge zone accessible for erosion (i.e., uplift rate lowers towards the final stages of fold growth by limb rotation; Poblet and Hardy, 1995; Poblet, 2004). When erosion thins or removes the hinge zones of salt-cored anticlines, the resulting differential loading with the adjacent synclinal troughs promotes salt flow inwards and toward the lower pressure core and hinge zone of the anticline. Then, piercing can take place when a critical overburden thickness is reached.

515

Some of these diapirism triggers have been invoked in the Eastern Romanian Carpathians fold-and-thrust belt, where the so called Moreni-Baicoi "salt lineament" constitutes a 30 km long squeezed diapir (i.e., Schleder et al., 2019; Tămaş et al. 2021). The formation of such salt diapir, aligned with the dominant NE-SW striking structural grain of the fold-and-thrust belt must have been favored by some kind of overburden weakening process or processes, since salt per se cannot pierce

520   trough the reported c.2-3km thick overburden originally burying the feeding salt horizon. In this sense, local extensional faulting in the transition from frontal to lateral thrust ramps was proposed by Munteanu et al. (2018), which is a plausible mechanism in the lateral terminations of arcuate thrust salients, such as that of the South-Central Pyrenees (Muñoz et al. 2013, 2024). Alternatively, Stefanescu et al. (2000) proposed that a middle-to-late Miocene (i.e., Meotian–Pontian in the local Para-Tethyan chronostratigraphy) extensional phase allowed for salt extrusion to the paleosurface. More recently,

525   Schleder et al. (2019) propose that a large erosional phase in between shortening phases (the large basal Meotian unconformity) deeply eroded the structural culminations of salt-cored detachment anticlines, allowing for the salt rise and flare onto the synorogenic paleosurface. These authors argue that no clear evidence for such phases of regional extension and thick-skinned left-lateral slip are present as proposed by Stefanescu et al (2000). The last deformations phase, according to these authors, rejuvenated and squeezed Carpathian salt structures.

530

Another interesting place for understanding the formation of purely contractional diapirs is the Sureste basin in the Gulf of Mexico (Sánchez Rivera et al. 2011; Davison, 2020). The Sureste basin displays one of the best examples of salt diapirs associated with contraction structures in a deep-water setting, with some salt-detached anticlines reaching astounding structural reliefs of more than 10km (e.g., Rowan et al. 2022). Large erosional peneplanations under deep water conditions

535   are highly unlikely in comparison to onshore shortening systems, and other processes must be responsible for diapirism to occur. In this area, the 3D interaction between detachment folding, thrust faulting, and salt diapirism is exceptionally constrained by seismic data and the key question is whether the salt diapirs predated the shortening or broke out during the contractional deformation. In their reported interpreted seismic sections, the hinges of upright detachment folds are thinned

by extensional faults (Rowan et al. 2022) where some of these crestal extensional faults are conjugate and dip inwards in
540 opposite senses, indicating outer arc extension accommodating concentric folding. Laterally, these faults pass into a series of
listric convex upwards extensional faults, suggesting extensional collapse of the anticline's crest as reported for other deep-
water gravity driven fold-belts (Morley, 2009). The interaction of detachment folding with thrusting and extensional
collapses are the main cause for the extrusion of salt a surface since large erosional events are highly unlikely.

545 In our Pyrenean scenario, an additional process has contributed fundamentally in the formation and evolution of the Mediano
anticline and the Clamosa diapir. Beside erosion, localized extensional faulting has also promoted thinning of the
overburden. The youngest structures are extensional faults (Teixell and Barnolas, 1995; Fernández, 2004) with a variable
trend from N–S to E–W. The most prominent one has a curvilinear map pattern and a throw of about 1 km that cuts the
Montsec-Peña Montañesa thrust sheet and the Gavarnie thrust sheet below (the Balupor-San Marzial fault; Fernández, 2004).
550 Extensional faults of this system obliquely truncate several anticlines of the Aínsa oblique zone and are spatially associated
with extensive Triassic outcrops. In cross section, these extensional faults appear as collapse features of the anticlines as they
partially reactivate their related thrusts at depth (e.g., Tavani et al. 2006). Since these extensional faults control along-strike
changes in the geometry of anticlines their occurrence suggests some synchronicity with fold growth (Fernández et al., 2012)
and are known to be active at least until Priabonian times since these faults offset late Eocene sediments. The extensional
555 faults defining the southern boundary of the Mediano anticline and the Clamosa diapir are similar in nature to the Balupor-
San Marzial fault in that they both are interpreted to be contained entirely within the Gavarnie thrust sheet. The extensional
faults are active until the Oligocene at least, since they cut through sediments of that age, and crosscut the entirety of the
Mediano anticline. Furthermore, the Balupor-San Marzial and the Clamosa faults are located where the N–S striking Aínsa
oblique structures swing to a NW–SE trend northwards in the case of the Balupor-San Marzial and southwards in the case of
560 Clamosa.

The origin of these extensional features relates to the contractional phase concomitant with the clock-wise vertical axis
rotation of the Aínsa Oblique Zone (Fig. 4). Paleomagnetic data from the N–S trending structures of the Aínsa Oblique Zone
reveals the kinematics of the South-Central Pyrenees thrust salient (Mochales et al., 2012, Muñoz et al., 2013). These
565 structures experienced clockwise vertical axis rotations that vary from 70° in the Mediano anticline to 55° further to the west.
Rotations of about 60°-45° occurred from early Lutetian to late Bartonian when the Clamosa diapir and Mediano anticline
developed. Rotation was partially accommodated by squeezing of a salt inflated area, the oblique to strike-slip reactivation
of former thrusts, and by the formation of new extensional faults, all these contributing to the thinning of the overburden and
diapirism, as indicated by the spatial association of these faults to outcrops of Triassic evaporites. In the case of the Mediano
570 anticline, rotation progressively diminished as recorded by its growth strata. Starting during the early Lutetian, the decrease
in the amount of rotation has been observed from 47.5 Ma onward. Syn-folding rotation continued at a decreasing rate at
least into the Priabonian. This vertical axis rotation stage resulted from a difference of about 50 km in the amount of

displacement on the Gavarnie thrust and an accompanying change in structural style at crustal scale from the central to the western Pyrenees. Such change has been interpreted originally as related to the NE–SW trending pinch out of Triassic
575 evaporites at its basal (Muñoz et al. 2013), and has been recently tested as well by means of sandbox analogue models (Muñoz et al. 2024).

6. Conclusions

580 The northwestern termination of the South-Central Pyrenean Salient serves as an outstanding scenario that exemplifies the evolution of purely contractional diapirs. First, syn-growth sediments provide an excellent dating tool for deciphering the structural evolution within areas tens of kilometres wide. As discussed, the formation of the Clamosa diapir responds to a combination of multiple factors that can be taken as a rule of thumb for diapir initiation and evolution within contractional settings. These include: the occurrence of a thick salt accumulation relative to is sedimentary overburden previous to the
585 onset of shortening, the inflation of it upon shortening and a series of concomitant processes that thin this overburden to the point that salt can pierce through it. These can be folding, uplift, and thinning of the overburden, either produced by erosion or local extensional faulting. Conversely, in the La Fueba system 15 km to the north of the Clamosa diapir, thin or absent salt, thrust stacking and moderate to high syncontractional sedimentation led to the formation of a contractional thrust system instead. The Mediano anticline could be considered as an intermediate member in which salt accumulated in its core, but
590 erosion was not significant enough to expose it. All in all, the Clamosa diapir, the Mediano anticline and the La Fueba thrust system illustrates how along strike changes in salt and cover thicknesses, thrust stacking and erosion-sedimentation processes lead to lateral variations that may trigger or hinder diapirism in contractional settings Examples from other contractional settings such as the Eastern Romanian Carpathians and the Sureste basin of Mexico suggest a key role of regional erosional episodes in the flaring and extrusion of salt from the cores of detachment anticlines, or the extensional
595 faulting to accommodate folding, or due to gravitational collapses of hinges and flanks in promoting diapirs under contraction regimes.

7. Appendix A. Bioestratigraphy samples

600   FIGURE A1
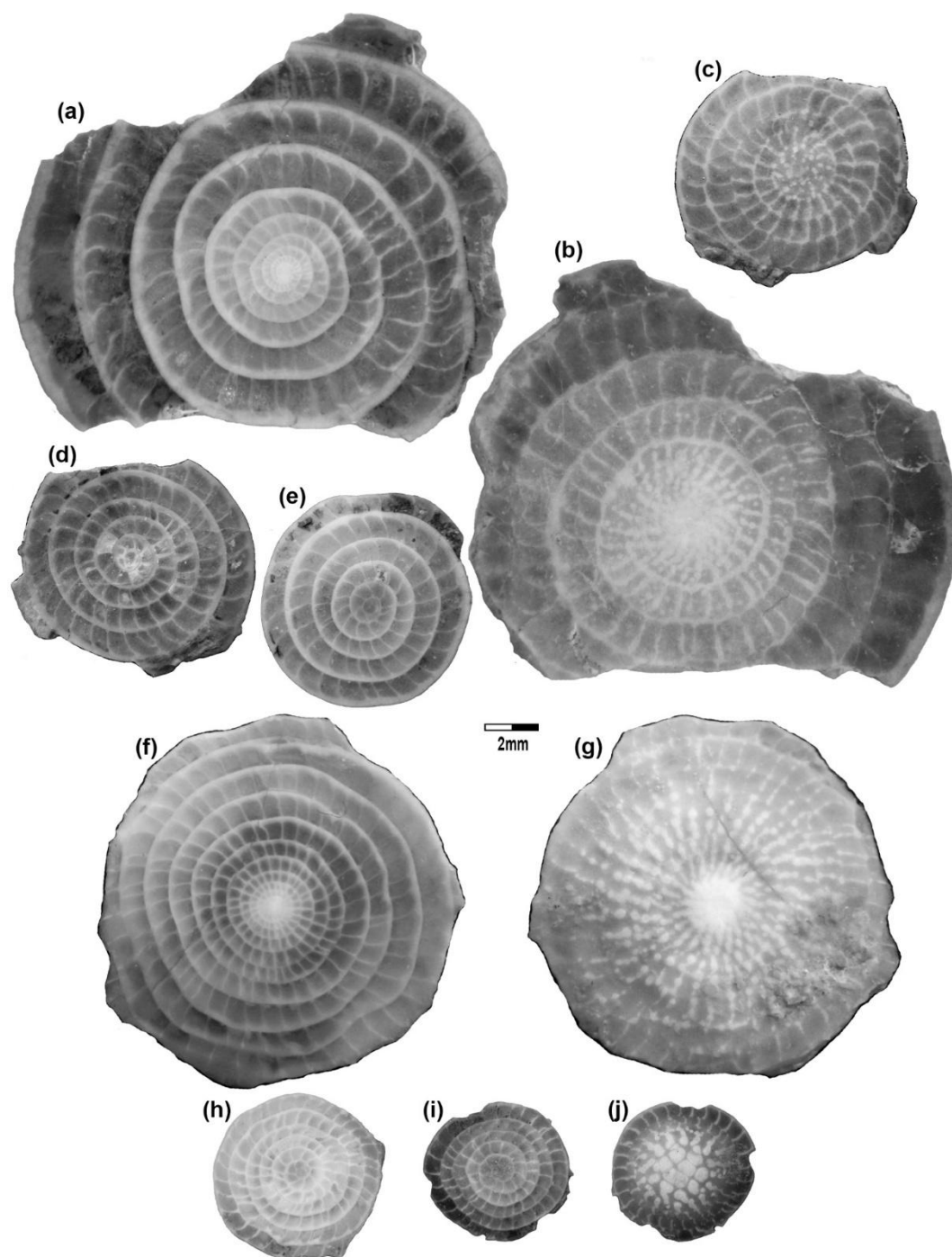
FIGURE A2
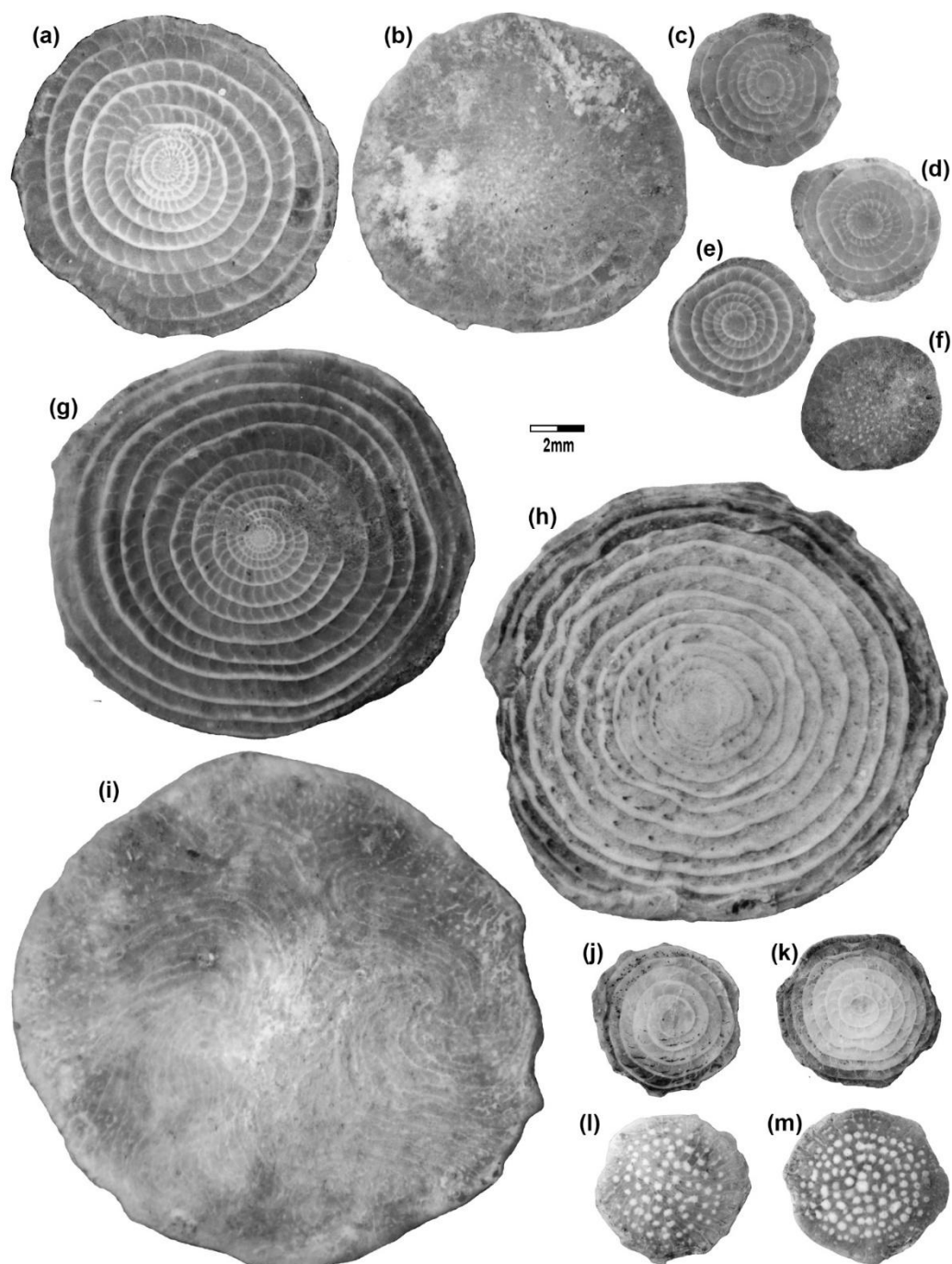
FIGURE A3
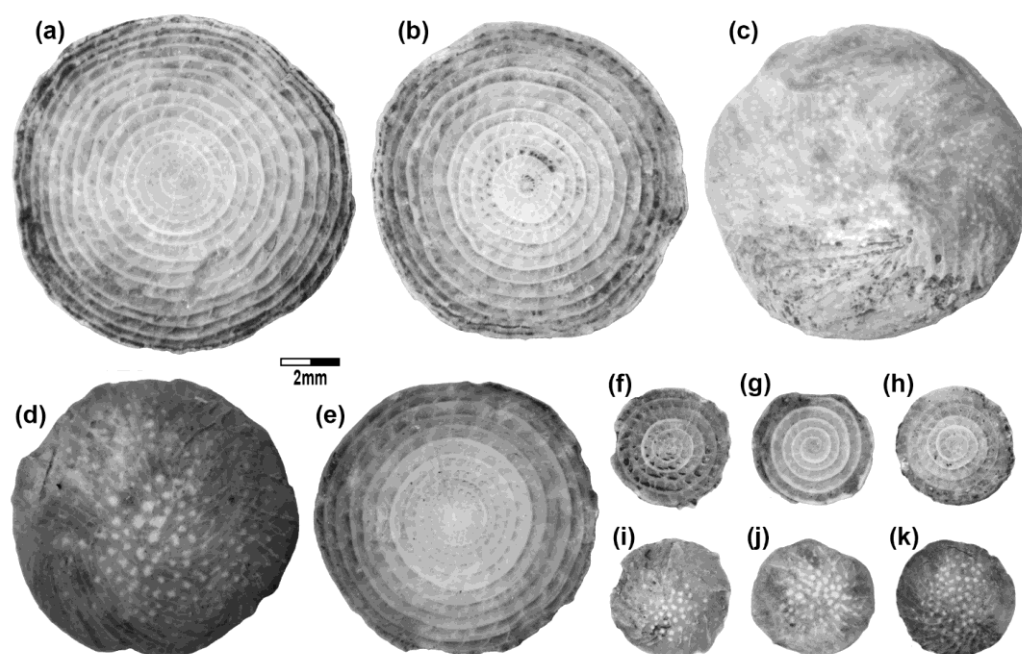
Figure captions:

Fig. A1: *Assilina maior* (a – e) and *A. cuvillieri* (f – j) a) *A. maior,* B form, equatorial section. b) *A. maior*, B form, external view. c) *A. maior,* A form, external view. d) and e) *A. maior,* A form, equatorial section. f) *A. cuvillieri*, B form, equatorial section. g) *A. cuvillieri*, B form, external view. h) and i). *A. cuvillieri*, A form, equatorial section. j) *A. cuvillieri*, A form, external view. All samples from **sample ST-1**. All samples 5x.

Fig. A2: *Nummulites manfredi* (a - f) and *N.* aff. *boussaci* (g - m). a) *N. manfredi,* B form, equatorial section. b) *N. manfredi,* B form, external view. c) and e) *N. manfredi,* A form, equatorial sections. f) *N. manfredi,* A form, external view. g) and h): *N.* aff. *boussaci,* B form, equatorial sections. (i): *N.* aff. *boussaci,* B form, external view. j) and k) *N.* aff. *boussaci,* A form, equatorial sections. l) and m) *N.* aff. *boussaci,* A form, external views. **Samples a) – f)** from **sample LP-1**, **samples g) – m)** from **sample Cb-4**. All samples 5x.

Fig. A3: *Nummulites campesinus.* a) and b) *N. campesinus,* B form, equatorial sections. c) and d) *N. campesinus,* B form, external views. d) *N. campesinus,* B form, equatorial section. f – h) *N. campesinus,* A forms, equatorial sections. i – k) *N. campesinus,* A form, external views. **All samples** from **sample ST-1**. All samples 5x.

625

Data Availability Statement

Seismic reflection profiles for this research are available and freely accessible in the SIGEOF repository, the Geophysical Information System of the IGME (Spanish Geological Survey). To access the data, use the web application (info.igme.es/SIGEOF/).

630

Author contribution

P.S.: Conceptualization, Methodology, Formal analysis, Investigation, Writing - Original Draft, Writing - Review & Editing

R.S.: Methodology, Formal analysis, Investigation, Writing - Review & Editing

N.C.: Formal analysis, Investigation, Writing - Review & Editing

635   J.AM.: Conceptualization, Formal analysis, Project administration, Writing - Review & Editing

P.A.: Formal analysis, Investigation, Writing - Review & Editing

P.G.: Writing - Review & Editing

Competing interest

640   The authors declare that they have no conflict of interest.

Acknowledgements

This is a contribution of the Institut de Recerca Geomodels. We acknowledge the support of the research project Structure and Deformation of Salt-bearing Rifted Margins (SABREM), PID2020-117598GB-I00, funded by MCIN/ AEI /10.13039/501100011033. Petroleum Experts are also acknowledged for providing Move software.

645   **References**

Arbués, P., D. Mellere, O. Falivene, O. Fernández, J. A. Muñoz, Marzo, M. and de Gibert, J. M., (2007). Context and architecture of the Ainsa-1-quarry channel complex, Spain, in T. H. Nilsen, R. D. Shew, G. S. Steffens, and J. R. J. Studlick, eds., Atlas of deep-water outcrops: AAPG Studies in Geology 56, CD-ROM, 20 pp.

Barnolas, A., Samsó, J. M., Teixell, A., Tosquella, J. and Zamorano, M., (1991). Evolución sedimentaria entre la cuenca de

650   Graus-Tremp y la cuenca de Jaca-Pamplona, in Colombo, F., ed., I Congreso el Grupo Español del Terciario: Libro-Guía de la Excursión 1: EUMO Gràfi c, Vic, Spain, 123 pp.

Barnolas, A., Teixell, A., García Senz, J., and Ramirez, J. I., (1994a). Mapa Geológico de España. 1:50000, Hoja 288, Fonz, IGME.

Barnolas, A., Teixell, A., Zamorano, M. and Ramirez, J. I., (1994b). Mapa Geológico de España. 1:50000, Hoja 250, Graus,

655   IGME.

Barnolas, A., Robador Moreno, A., Zamorano, M. (1999). Mapa Geológico de España. 1:50000, Hoja 212, Campo, IGME.

Barrier, L., Nalpas, T., Gapais, D. and Proust, J. N., (2013). Impact of synkinematic sedimentation on the geometry and dynamics of compressive growth structures: Insights from analogue modelling. Tectonophysics 608, 737-752.

Beamud Amorós, E. (2013). Paleomagnetism and thermochronology in tertiary syntectonic sediments of the south-central
660 Pyrenees: chronostratigraphy, kinematics and exhumation constraints. Tesis Doctoral, Univ. Barcelona, 251 pp.

Bentham, P. A. and Burbank, D. W. (1996). Chronology of Eocene foreland basin evolution along the western oblique margin of the South-Central Pyrenees, in Tertiary basins of Spain, edited by P. F. Friend and C. J. Dabrio, Cambridge University Press, 144-152.

Bonini, M. (2003). Detachment folding, fold amplification, and diapirism in thrust wedge experiments. Tectonics 22, 1065-
665 1103.

Callot, J. P., Trocmé, V., Letouzey, J., Albouy, E., Jahani, S. and Sherkati, S. (2012). Pre-existing salt structures and the folding of the Zagros Mountains. In, Alsop, G. I., Archer, S. G., Hartley, A. J., Grant, N. T. and Hodgkinson, R. (eds) 2012. Salt Tectonics, Sediments and Prospectivity. Geological Society, London, Special Publications 363, 545–561. http://dx.doi.org/10.1144/SP363.27

670 Calvín, P., Casas-Sainz, A.M., Villalaín, J.J., Moussaid, B., 2018. Extensional vs. compressional deformation in the Central High Atlas salt province: a paleomagnetic approach. Tectonophysics 130–147. https://doi.org/10.1016/j.tecto.2018.04.007, 734–735.

Cámara, P. and Klimowitz, J. (1985). Interpretación geodinámica de la vertiente centro-occidental surpirenaica (Cuencas de Jaca-Tremp). Estudios geológicos 41, 391-404.

675 Campanyà, J., Ledo, J., Queralt, P., Marcuello, A., Liesa, M. and Muñoz, J. A. (2012). New geoelectrical characterisation of a continental collision zone in the West-Central Pyrenees: Constraints from long period and broadband magnetotellurics. Earth and Planetary Science Letters 333-334, 112-121

Canérot, J., Hudec, M.R., Rockenbauch, K., 2005. Mesozoic diapirism in the Pyrenean orogen: Salt tectonics on a transform plate boundary. AAPG Bulletin, 89, 211-229.

680 Canova, D.P., Roca, E., Ferrer, O., Ferràndez-Cañadell, C., Escosa, F.O., Afzal, J., 2025. From salt carapace to secondary minibasin encasement—The Bolon Secondary Minibasin, Eastern External Betics SE Iberia. https://dx.doi.org/10.2139/ssrn.5095927

Casas-Sainz, A.M., Villalaín. J.J., Román-Berdiel, T., Calvín, P., Marcén, M., Izquierdo-Llavall, E., Santolaria, P., Pocoví, A., Mochales, T., Oliva-Urcia, B., El-Ouardi, H., Moussaid, 2023. Structure of the Central High Atlas (Morocco).
685 Kinematics of Structures and Basin Evolution in the Central High Atlas. Constraints from AMS and Paleomagnetic Data. In: Tectonic Evolution of the Moroccan High Atlas: A Paleomagnetic Perspective, eds. Calvín, P., Casas-Sainz, A.M., Román-Berdiel, T., Villalaín, J.J., Springer Geology, pp. 487-646

Célini, N., Callot, J.-P., Ringenbach, J.-C., Graham, R., 2020. Jurassic salt tectonics in the SW sub-alpine fold-and-thrust belt. Tectonics 39 (10). https://doi.org/10.1029/2020TC006107, 47–36.

690   Chevrot, S., Sylvander, M., Díaz, J., Martin, R., Mouthereau, F., Manatschal, G., Masini, E., Calassou, S., Grimaud, F., Pauchet, H. and Ruiz, M. (2018). The non cylindrical crustal architecture of the Pyrenees. Scientific Reports 8(1), 9591pp. http://doi.org/10.1038/s41598-018-27889-x

Chevrot, S., Sylvander, M., Diaz, J., Ruiz, M., Paul, A. and the PYROPE Working Group (2015) The Pyrenean architecture as revealed by teleseismic P-to-S converted waves recorded along two dense transects. Geophysical Journal International,

695   200(2), 1094–1105. doi:10.1093/gji/ggu400

Choukroune, P., (1989). The ECORS Pyrenean deep seismic profile reflection data and the overall structure of an orogenic belt. Tectonics 8 (1), 23-39.

Costa, E., and Vendeville, B. C. (2002). Experimental insights on the geometry and kinematics of fold-and-thrust belts above a weak, viscous evaporite décollement. Journal of Structural Geology 24 (11), 1729-1739.

700   Cotton, J. T. and Koyi, H. A. (2000). Modeling of thrust fronts above ductile and frictional detachments: Application to structures in the Salt Range and Potwar Plateau, Pakistan. Geol. Soc. Amer. Bull. 112, 351-363.

Davis, D. M. and Engelder, T. (1985). The role of salt in fold and thrust belts and accretionary wedges: cohesive Coulomb theory. Journal of Geophysical Research, 89, 10087-10101.

Davison, I., 2020. Salt tectonics in the Sureste Basin, SE Mexico: some implications for hydrocarbon exploration. In:

705   Davison, I., Hull, J.N.F., Pindell, J. (Eds.), The Basins, Orogens and Evolution of the Southern Gulf of Mexico and Northern Caribbean. Geol. Soc., vol. 504 Spec. Pub, London. https://doi.org/10.1144/SP504-2019-227.

De Federico, A., (1981). La sedimentación de talud en el sector occidental de la cuenca paleógena de Ainsa: Bellaterra, Universitat Autònoma de Barcelona, Publicacions de Geologia, v. 12, 271 p.

Dooley, T.P., Jackson, M.P.A., Hudec, M.R., 2009. Inflation and deflation of deeply buried salt stocks during lateral

710   shortening. J. Struct. Geol. 31, 582–600. https://doi. org/10.1016/j.jsg.2009.03.013.

Duerto, L. and McClay, K. (2009). The role of syntectonic sedimentation in the evolution of doubly vergent thrust wedges and foreland folds. Marine and Petroleum Geology 26(7), 1051–1069.

Escosa, F.O., Roca, E., Ferrer, O., 2018. Testing thin-skinned inversion of a prerift salt-bearing passive margin (Eastern Prebetic Zone, SE Iberia). Journal of Structural Geology, 109, 55-73.

715   Fernández, O., Muñoz J. A., Arbués, P. and Falivene, O. (2012). 3D Structure and evolution of an oblique system of relaying folds: The Ainsa basin (Spanish Pyrenees). Journal of the Geological Society of London 169, 545-559.

Fernández, O., Muñoz, J. A., Arbués, P., Falivene, O., Marzo, M. (2004). Three-dimensional reconstruction of geological surfaces: An example of growth strata and turbidite systems from the Ainsa basin (Pyrenees, Spain). AAPG Bulletin, 88(8), 1049-1068.

720   Fernández-Bellón, O. (2004). Reconstruction of geological structures in 3D. An example from the Southern Pyrenees. Ph.D. thesis, Universitat de Barcelona, 321 pp.

Fernández, O., Ortner, H., Sanders, D., Grasemann, B., Leitner, T., 2024. Salt-rich versus salt-poor structural scenarios in the central Northern Calcareous Alps: implications for the Hallstatt facies and early Alpine tectonic evolution (Eastern Alps, Austria). International Jorunal of Earth Sciences, https://doi.org/10.1007/s00531-023-02377-4

Fillon, C., Huismans, R. S., van der Beek, P. and Muñoz, J. A. (2013). Syntectonic sedimentation controls on the evolution of the southern Pyrenean fold-and-thrust belt: Inferences from coupled tectonic-surface processes models. Journal of geophysical research: Solid Earth, 118, 1-16.

Flinch, J.F., Soto, J.I. (2022). Structure and Alpine tectonic evolution of a salt canopy in the western Betic Cordillera (Spain). Marine and Petroleum Geology 143, 105782, https://doi.org/10.1016/j.marpetgeo.2022.105782.

Franco-Balaguer, J., Casas Sainz, A.M. (2016): Estructura de la terminación occidental del cabalgamiento del Montsec (Pirineos Centrales). Revista de la Sociedad Geológica de España, 29(2): 39-55.

Garrido-Megías, A. (1968). Sobre la estratigrafía de los conglomerados de Campanué (Santa Liestra) y formaciones superiores del Eoceno (extremo occidental de la cuenca de TrempGraus, Pirineo central, provincia de Huesca). Acta. Geol. Hispánica, 3, pp. 39-43.

Garrido-Megías, A. (1973). Estudio geológico y relación entre tectónica y sedimentación del Secundario y Terciario de la vertiente meridional pirenaica en su zona central (Provincias de Huesca y Lérida). PhD thesis, Universidad de Granada, 395pp.

Garrido-Megías, A., Rios-Aragües, L.M. (1972). Síntesis geológica del Secundario y Terciario entre los ríos Cinca y Segre (Pirineo central de la vertiente sur pirenaica, provincias de Huesca y Lérida). Boletín Geológico y Minero, 83, 1-47.

Gomis, L. E., López-Blanco, M., Vidal, I. and Serra-Kiel, J. (2012). Arquitectura y distribución de sedimentos marinos someros y de talud influenciados por el crecimiento de pliegues sinsedimentarios (Abizanda, Luteciense medio, Zona Surpirenaica Central). VIII Congreso Geológico de España. Geo-Temas 13, 106.

Gradstein, F.M., Ogg, J.G., Schmitz, M.D., Ogg, G.M., 2020. Geologic Time Scale 2020. Elsevier, 1357pp, https://doi.org/10.1016/C2020-1-02369-3

Granado, P., Santolaria, P., Muñoz, J.A., 2023 Interplay of downbuilding and gliding in salt-bearing rifted margins: insights from analogue modelling and natural case studies. AAPG Bulletin, 107, 12, 2091-2118, DOI:10.1306/08072221203.

Granado, P., Roca, E., Strauss, O., Pelz, K., Muñoz, J.A. (2019). Structural styles in fold-and-thrust belts involving early salt structures: The Northern Calcareous Alps (Austria). Geology 47(1), 51-54. doi: 10.1130/G45281.1

Granado, P., Ruh, J.B., Santolaria, P., Strauss, P., Muñoz, J.A. (2021). Stretching and Contraction of Extensional Basins With Pre-Rift Salt: A Numerical Modeling Approach. Frontiers in Earth Science 9, https://doi.org/10.3389/feart.2021.648937

Harrison, J. C. (1995). Tectonics and kinematics of a foreland folded belt influenced by salt, Arctic Canada. In M. P. A. Jackson, D. G. Roberts, and S. Snelson, eds., Salt tectonics: a global perspective. AAPG Memoir 65, 379-412.

Heim, A. (1908). Die Nummuliten- und Flyschbildungen der Schweizeralpen, Versuch zu einer Revision der alpinen Eocaen-Stratigraphie. Abhandlungen Der Schweizerischen Paläontologischen Gesellschaft, vol. 35: 1–330

Holl, J. E., and Anastasio, D. J. (1993). Paleomagnetically derived folding rates, southern Pyrenees, Spain. Geology 21, 271-274 pp.

Hudec, M.R., Dooley, T.P., Burrel, L., Teixell, A., Fernandez, N., 2021. An alternative model for the role of salt depositional configuration and preexisting salt structures in the evolution of the Southern Pyrenees, Spain. Journal of Structural Geology 146, 104325. https://doi.org/10.1016/j.jsg.2021.104325

Izquierdo-Llavall, E., Roca, E., Xie, H., Pla, O., Muñoz, J. A., Rowan, M. G., Yuan, N. and Huang, S. (2018). Influence of Overlapping décollements, Syntectonic Sedimentation, and Structural Inheritance in the Evolution of a Contractional System: The Central Kuqa Fold-and-Thrust Belt (Tian Shan Mountains, NW China). Tectonics, https://doi.org/10.1029/2017TC004928

Jackson, M. P. A. and Vendeville, B. C. (1994). Regional extension as a geologic trigger for diapirism. GSA Bulletin 106, 57–73.

Jahani, S., Callot, J. P., Letouzey, J., Frizon De Lamotte, D., 2009. The eastern termination of the Zagros Fold-and-Thrust Belt, Iran: Structures, evolution, and relationships between salt plugs, folding, and faulting. Tectonics, 28 (6), TC6004 doi:10.1029/2008TC002418.

López-Gómez et al., 2019 In: C. Quesada and J. T. Oliveira (eds.), The Geology of Iberia: A Geodynamic Approach, Regional Geology Reviews. Springer Nature Switzerland AG 2019 https://doi.org/10.1007/978-3-030-11295-0_3

Martínez-Peña, M. B. and Casas-Sainz, A. M. (2003). Cretaceous-Tertiary tectonic inversion of the Cotiella Basin (Southern Pyrenees, Spain). International Journal of Earth Sciences (Geol. Rundsch.) 92, 99-113.

Mateu-Vicens, G., Pomar, L. and Ferrández, C. (2012). Nummulitic banks in the upper Lutetian "Buil level", Ainsa Basin, South Central Pyrenean Zone: The impact of internal waves, Sedimentology 59(2), 527–552.

Mey, P. H. W., P. J. C. Nagtegaal, K. J. Roberti, and J. J. A. Hartevelt (1968). Lithostratigraphic subdivision of post-Hercynian deposits in the south-central Pyrenees, Spain, Leidse Geologische Mededelingen, 431, 221–228

Mitra, S. (2002) Fold-Accommodation Faults. AAPG Bulletin 86 (4), 671–693.

Mitra, S. 2003. A unified kinematic model for the evolution of detachment folds. Journal of Structural Geology 25, 1659-1673.

Mochales, T., Casas, A.M., Pueyo, E.L., Barnolas, A., 2012. Rotational velocity for oblique structures (Boltaña anticline, Southern Pyrenees). J. Struct. Geol. 35, 2–16.

Morley, C.K. (2009) Growth folds in a deep water setting. Geosphere 5 (2), 59–89. doi: 10.1130/GES00186.1

Mugnier, J. L., Baby, P., Colletta, B., Vinour, P., Bale, P., Leturmy, P., 1997. Thrust geometry controlled by erosion and sedimentation: a view from analogue models. Geology 25(5), 427-430.

Munteanu I, Garcia A, Dobre S, Tilita M, Vasiliu M, Fernandez O, Matias H, Tulucan A, Cascone L, Escandell F, Garcia Gomez, M (2018) Lateral ramps and salt diapirism in the Diapiric Fold Zone of Romania. AAPG Granada, Workshop 2018

Muñoz, J. A. (1992). Evolution of a continental collision belt: ECORS-Pyrenees crustal balanced cross section. In: Thrust tectonics, (K. R. McClay, ed.), Chapman & Hall, Londres, 235-246.

Muñoz, J. A., Beamud, E., Fernández, O., Arbués, P., Dinarès-Turell, J. and Poblet, J. (2013). The Ainsa Fold and Thrust Oblique Zone of the Central Pyrenees: kinematics of a curved contractional system from paleomagnetic and structural data. Tectonics 32(5), 1142-1175.

Muñoz, J. A., Mencos, J., Roca, E., Carrera, N., Gratacos, O., Ferrer, O. and Fernandez, O. (2018). The structure of the South-Central Pyrenean fold and thrust belt as constrained by subsurface data. Geologica Acta: an International Earth Science Journal 16(4), 439–460. http://doi.org/10.1344/GeologicaActa2018.16.4.7

Muñoz, J.A., Ferrer, O., Gratacós, O., Roca, R., 2024. The influence of the geometry of salt detachments on thrust salient development: An analogue modelling approach based on the South-Central Pyrenean thrust salient. Journal of Structural Geology, 105078, https://doi.org/10.1016/j.jsg.2024.105078

Nijman, W., Nio, S.D. (1975). The Eocene Montañana delta. In: J. Rosell and Puigdefábregas (Eds.), Sedimentary evolution of the Paleogene South Pyrenean Basin. IAS 9th International Congress, Nice, part B, 56 p.

Nijman, W., Puigdefàbregas, C., 1978. Coarse-grained point bar structure in a molasse-type system, Eocene Castissent Formation, South Pyrenean Basin. In: Fluvial Sedimentology (Ed. A.D. Miall). Mem. Can. Soc. Petrol. Geol., 5, 487-510.

Pedreira, D., Pulgar, J. A., Gallart, J. and Díaz, J. (2003). Seismic evidence of Alpine crustal thickening and wedging from the western Pyrenees to the Cantabrian Mountains (north Iberia). Journal of Geophysical Research: Solid Earth 108(B4), 2204. doi:10.1029/2001JB001667

Pichot, T. and Nalpas, T. (2009). Influence of synkinematic sedimentation in a thrust system with two decollement levels; analogue modelling. Tectonophysics 473, 466-475.

Plaziat, J.C., (1984), Le domaine Pyrénéen de la fin de Crétacé a la fin de l'Eocene. Stratigraphie, paléoenvironments et évolution paléogeographique. PhD Thesis. Université de Paris-sud, 1362p.

Poblet, J., Muñoz, J. A., Travé, A. and Serra-Kiel, J. (1998). Quantifying the kinematics of detachment folds using three-dimensional geometry: Application to the Mediano anticline (Pyrenees, Spain). Geological Society of America Bulletin 110(1), 111-125.

Ramirez-Perez, P., Cofrade, G., Martín-Martín, J.D., Travé, A., 2024. Stratigraphic evolution of a salt-walled basin: the influence of diapirism and compressional tectonics on the sedimentary record of the Estopanyà syncline (South-Central Pyrenees). Marine and Petroleum Geology, 163, 106715.

Roca, E., Sans, M., Koyi, H.A., 2006. Polyphase deformation of diapiric areas in models and in the Eastern Prebetics (Spain). AAPG Bull. 90, 115–136. http://dx.doi.org/10. 1306/07260504096.

Rodríguez-Pintó, A., Pueyo, E.L., Serra-Kiel, J., Barnolas, A., Samsó, J.M., Pocoví, A., 2013. The Ypresian–Lutetian boundary in the Southwestern Pyrenean Basin; magnetostratigraphy from the San Pelegrín section. Palaeogeography, Palaeoclimatology, Palaeoecology, 370, 13-29.

Rodríguez-Pintó, A., Pueyo, E.L., Serra-Kiel, J., Samsó, J.M., Barnolas, A., Pocoví, A., 2012. Lutetian magnetostratigraphic calibration of larger foraminifera zonation (SBZ) in the Southern Pyrenees: The Isuela Section. Palaeogeography, Palaeoclimatology, Palaeoecology, 333-334, 107-120.

Rodríguez-Pintó, A., Serra-Kiel, J., Bernaola, G., Barnolas, A., Pueyo, E.L., Tosquella, J., Arbués, P., Scholger, R., 2022.
825   The early/middle Eocene transition at the Ésera valley (South-Central Pyrenees): Implications in Shallow Benthic Zones
        (SBZ). Geologica Acta, 20.6, 1-25. DOI: 10.1344/GeologicaActa2022.20.6

Rowan, M. G. (2020). Salt- and shale-detached gravity-driven failure of continental margins. In N. Scarselli, J. Adam, D.

Rowan, M.G., Muñoz, J.A., Roca, E., Ferrer, O., Santolaria, P., Granado, P., Snidero, M. (2022). Linked detachment folds,
        thrust faults, and salt diapirs: Observations and analog models. Journal of Structural Geology 155, 104509.
830   https://doi.org/10.1016/j.jsg.2022.104509

Rowan, M.G., Vendeville, B.C., 2006. Foldbelts with early salt withdrawal and diapirism: physical model and examples
        from the northern Gulf of Mexico and the Flinders Ranges, Australia. Mar. Pet. Geol. 23 (9–10), 871–891.

Ruh, J. B., Kaus, B. J. P. and Burg, J. P. (2012). Numerical investigation of deformation mechanics in fold-and-thrust belts:
        Influence of rheology of single and multiple décollements. Tectonics 31, TC3005, doi:10.1029/2011TC003047

835   Sánchez Rivera, R., Cruz Mercado, M.A., Reyes Tovar, E., López Céspedes, H.G., Peterson Rodríguez, R.H., Flores
        Zamora, J.C., León Ramírez, R., Barrera González, D., (2011). Tectonic evolution of the south Gulf salt province in the Gulf
        of Mexico. Gulf Coast Assoc. Geol. Soc. Trans. 61, 421–427.

Sans, M., Koyi, H.A., 2001, Modeling the role of erosion in diapir development in contractional settings. Geological Society
        of America Memoir 193, p. 111-122

840   Santolaria, P., Casas-Sainz, A. M., Soto, R., Pinto, V., Casas, A, 2014. The Naval diapir (Southern Pyrenees): Geometry of a
        salt wall associated with thrusting at an oblique ramp. Tectonophysics, 637, 30-44.

Santolaria, P. (2015). Salt and thrust tectonics in the South Central Pyrenees. PhD thesis, University of Zaragoza, 327 pp.

Santolaria, P., Casas, A., Casas-Sainz, A. M. and Soto, R. (2016). Gravimetric modelling to assess salt tectonics in the
        western end of the south Pyrenean central unit. Journal of the Geological Society 174 (2), 269-288. doi: 10.1144/jgs2016-
845   027.

Santolaria, P., Ferrer, O., Rowan, M.G., Snidero, M., Carrera, N., Granado, P., Muñoz, J. A., Roca, E., Schneider, C.L., Piña,
        A., Zamora, G., 2021a. Influence of preexisting salt diapirs during thrust wedge evolution and secondary welding: insights
        from analog modeling. J. Struct. Geol. 149, 104374. https://doi.org/10.1016/j.jsg.2021.104374.

Santolaria, P., Granado, P., Carrera, N., Schneider, C.L., Ferrer, O., Snidero, M., Strauss, P., Pelz, K., Roca, E., Muñoz, J.A.,
850   2021b. From downbuilding to contractional reactivation of salt-sediment systems: Insights from analog modeling.
        Tectonophysics, 918, 229078, https://doi.org/10.1016/j.tecto.2021.229078.

Santolaria, P., Granado, P., Wilson, E. P., de Matteis, M., Ferrer, O., Strauss, P., et al. (2022). From salt-bearing rifted
        margins to fold-and-thrust belts. Insights from analog modeling and Northern Calcareous Alps case study. Tectonics, 41,
        e2022TC007503. https://doi.org/10.1029/2022TC007503

855   Saura, E., Vergés, J., Martín-Martín, J.D., Messager, G., Moragas, M., Razin, P., Grélaud, C., Joussiaume, R., Malaval, M.,
        Homke, S., 2014. Syn-to post-rift diapirism and minibasin of the Central High Atlas (Morocco): The changing face of a
        mountain belt. Journal of the Geological Society, 171, 97-105.

Schaub, H., 1966. Ueber die Grossforaminiferen im Untereocaen von Campo Ober-Aragonien). Eclogae Geologicae Helvetiae, 59, 355-377.

860 Schaub, H., 1981. Nummulites et Assilines de la Téthys Paléogène. Taxinomie, phylogénese et biostratigraphie. Mémoires suisses de paléontologie, 104-105-106, 236pp, 97pl.

Schleder, Z., Tămaş, D.M., Krezsek, C., Arnberger, K., Tulucan, A. (2019). Salt tectonics in the Bend Zone segment of the Carpathian fold and thrust belt, Romania. International Journal of Earth Sciences 108, 1595–1614

Schlumberger, C. (1905). Deuxième note sur les Miliolidées trématophorées. Bulletin de la Société géologique de France.
865 (série 4) 5 (2): 115-134

Séguret, M. (1972). Etude tectonique de nappes et series decollés de la partie central du versant sud des Pyrenées. Caractére sedimentaire rôle de la compression et de la gravité. Tesis doctoral, Univ. de Montpellier, 155 pp.

Serra-Kiel, J., Hottinger, L., Caus, E., Ferràndez, C., Jauhri, A.K., Less, G., Pavlovec, R., Pignatti, J., Samsó, J.M., Schaub, H., Sirel, E., Strougo, A., Tosquella, J., Zakrevskaya, E., 1998. Larger foraminiferal biostratigraphy of the Tethyan
870 Paleocene and Eocene. Bulletin de la Société géologique de France, 169(2), 281-299.

Snidero, Carrera, M. N., Mencos, J., Butillé, M., Granado, P., Tavani, S., Lopez-Mir, B., Sàbat, F., Muñoz, J. A., 2020. Diapir kinematics in a multi-layer salt system from the eastern Persian Gulf, Marine and Petroleum Geology, 117, 104402, ISSN 0264-8172.

Soto, R., Casas, A. M., Storti, F. and Faccenna, C. (2002). Role of lateral thickness variations on the development of oblique
875 structures at the western end of the South Pyrenean Central Unit, Tectonophysics 350, 215-235.

Stefanescu, M., Dicea, O., Tari, G. (2000) Influence of extension and compression on salt diapirism in its type area, East Carpathian Bend area, Romania. In: Vendeville BC, Mart Y, Vigneresse JL (eds) Salt, shale and igneous diapirs in and around Europe. Geological Society, London, pp 131–147. https ://doi.org/10.1144/GSL.SP.1999.174.01.08.

Stewart, S. A. (1999). Geometry of thin-skinned tectonic systems in relation to detachment layer thickness in sedimentary
880 basins. Tectonics 18, 719-732.

Storti, F., McClay, K.R. 1995. Influence of syntectonic sedimentation on thrust wedges in analogue models. Geology 23 (11): 999–1002. doi: https://doi.org/10.1130/0091-7613(1995)023<0999:IOSSOT>2.3.CO;2

Strauss, P., Granado, P., Muñoz, J.A., Böhm, K., Schuster, R., (2023). The Northern Calcareous Alps revisited: Formation of a hyperextended margin and mantle exhumation in the Northern Calcareous Alps sector of the Neo-Tethys (Eastern Alps,
885 Austria). Earth-Science Reviews, 243, 104488, https://doi.org/10.1016/j.earscirev.2023.104488

Tavani, S., Storti, F., Fernández, O., Muñoz, J.A., Salvini, F. (2006). 3-D deformation pattern analysis and evolution of the Añisclo anticline, southern Pyrenees. Journal of Structural Geology 28 (4), 695-712.

Teixell, A. (1996). The Ansó transect of the southern Pyrenees: basement and cover thrust geometries. J. Geol. Soc. London 153, 301-310.

890 Teixell, A. and Barnolas, A. (1995). Significado de la discordancia de Mediano en relación con las estructuras adyacentes (Pirineo central). Geogaceta 17, 186-189.

Teixell, A., Labaume, P., Ayarza, P., Espurt, N., de Saint Blanquat, M., Lagabrielle, Y. (2018). Crustal structure and evolution of the Pyrenean-Cantabrian belt_ A review and new interpretations from recent concepts and data. Tectonophysics 724-725, 146–170. http://doi.org/10.1016/j.tecto.2018.01.009

895   Vakalas, I.; Kokkalas, S.; Konstantopoulos, P.; Tzimeas, C.; Kampolis, I.; Tsiglifi, H.; Pérez-Martin, R.; Hernandez-Jiménez, P.; Pita-Gutierrez, J.P. Implications of Salt Diapirism in Syn-Depositional Architecture of a Carbonate Margin-to-Edge Transition: An Example from Plataria Syncline, Ionian Zone, NW Greece. Appl. Sci. 2023, 13, 7043. https://doi.org/10.3390/app13127043

Velaj, T. Evaporites in Albania and their impact on the thrusting processes. Carbonates Evaporites 2002, 17, 68–78.

900   Vendeville, B. C. and Jackson, M. P. A. (1992). The rise of diapirs during thin-skinned extension. Marine and Petroleum Geology 9, 331–353.

Vendeville, B.C., Nilsen, K.T., 1995. Episodic growth of salt diapirs driven by horizontal shortening. In: Travis, C.J., Harrison, H., Hudec, M.R., Vendeville, B.C., Peel, F.J., Perkins, B.F. (Eds.), Salt, Sediment, and Hydrocarbons. SEPM Gulf Coast Section 16th Annual Research Foundation Conference, pp. 285–295.

905   Wiltschko, D.V., and Chapple, W.M., 1977. Flow of weak rocks in Appalachian Plateau folds: American Association of Petroleum Geologists Bulletin,v. 61, p. 653–670.